

Phonon hydrodynamics for nanoscale heat transport at ordinary temperatures

Yangyu Guo and Moran Wang*

*Key Laboratory for Thermal Science and Power Engineering of the Ministry of Education,
Department of Engineering Mechanics and CNMM, Tsinghua University, Beijing 100084, China*

(Received 14 November 2017; published 16 January 2018)

The classical Fourier's law fails in extremely small and ultrafast heat conduction even at ordinary temperatures due to strong thermodynamic nonequilibrium effects. In this work, a macroscopic phonon hydrodynamic equation beyond Fourier's law with a relaxation term and nonlocal terms is derived through a perturbation expansion to the phonon Boltzmann equation around a four-moment nonequilibrium solution. The temperature jump and heat flux tangential retardant boundary conditions are developed based on the Maxwell model of the phonon-boundary interaction. Extensive steady-state and transient nanoscale heat transport cases are modeled by the phonon hydrodynamic model, which produces quantitative predictions in good agreement with available phonon Boltzmann equation solutions and experimental results. The phonon hydrodynamic model provides a simple and elegant mathematical description of non-Fourier heat conduction with a clear and intuitive physical picture. The present work will promote deeper understanding and macroscopic modeling of heat transport in extreme states.

DOI: [10.1103/PhysRevB.97.035421](https://doi.org/10.1103/PhysRevB.97.035421)**I. INTRODUCTION**

With the rapid development of advanced technologies in recent years, there have been extensive studies on extremely small and ultrafast heat conduction [1–3]. The exploration of lowly and highly thermal conductive nanomaterials respectively for thermoelectric [4,5] and micro/nanoelectronics cooling [6,7] applications requires a deeper understanding of the heat conduction at an extremely small spatial scale. On the other hand, the short-pulse laser heating machining [8,9] involves the mechanism of heat conduction during an ultrafast time scale. The classical Fourier's law is no longer valid in these systems and processes due to strong thermodynamic nonequilibrium effects, as the characteristic length and time become comparable to or smaller than the mean-free path and relaxation time of heat carriers.

To treat non-Fourier heat conduction, there have been usually three categories of theoretical approaches: microscopic, mesoscopic, and macroscopic methods [3]. The microscopic method mainly includes the *ab initio* (first-principles) calculation [10,11] and molecular dynamics simulations [12,13], which are usually limited to relatively small structures and simple systems. The current main trend is the mesoscopic method based on a solution of phonon Boltzmann equation supplemented with phonon properties from microscopic methods [14–17]. In spite of much progress in microscopic and mesoscopic modeling of non-Fourier heat conduction, researchers have not stopped looking for a macroscopic description based on a heat transport equation similar to Fourier's law [18–21]. Macroscopic methods provide not only a clear and intuitive physical picture, but also an elegant and unified mathematical description. Among the existing branches of macroscopic methods, the phonon hydrodynamic model is the

most promising one since it is a natural and direct production from the phonon Boltzmann equation [3].

The study of phonon hydrodynamics began in the middle years of the last century during the exploration of heat waves in dielectric crystals [22]. The Guyer-Krumhansl (G-K) phonon hydrodynamic equation was derived from the phonon Boltzmann equation with the eigenvalue analysis method [23,24], and later obtained in the framework of nine-moment phonon hydrodynamics [25,26] and the Chapman-Enskog expansion [3]; however it is merely restricted to the low-temperature situation where nonresistive phonon normal scattering plays a major role. To meet situations in actual applications, the G-K equation has been recently adapted to model non-Fourier heat conduction in nanostructures often at ordinary temperatures through an analogy between phonon flow and high-Knudsen-number gas flow [19]. The phonon hydrodynamic model provides an effective approach to understand heat conduction in nanosystems from the fluid mechanical perspective [27–30], and has also been verified to be compatible with the second law in extended irreversible thermodynamics [31–34]. Yet there still exists a theoretical gap between this phenomenological phonon hydrodynamic model and more fundamental phonon kinetic theory as the resistive phonon scattering mostly dominates at ordinary temperatures [3,35]. On the other hand, the heat flux boundary condition for the G-K equation was directly borrowed from the velocity slip boundary condition for high-Knudsen-number gas flow neglecting the difference between phonons and molecules [19]. Some efforts have been made to derive macroscopic heat transport equations from the phonon Boltzmann equation based on a hypothetical division of the phonon spectrum into a ballistic part and diffusive part [36–38]. A Hilbert-like asymptotic solution is given to the phonon Boltzmann equation around the equilibrium distribution [39], where the near-continuum heat transport with kinetic effects by boundary inhomogeneity is modeled via the extended Fourier's description with jump-type boundary conditions and Knudsen

*Corresponding author: mrwang@tsinghua.edu.cn

layer corrections. This continuum model does not treat the kinetic effects in a spatially homogeneous material with temporal and spatial thermal variations at a characteristic dimension comparable to or even smaller than the phonon relaxation time and mean-free path [39]. The classical maximum entropy moment method is applied to derive macroscopic equations for phonon heat transport at room temperature in a recent study [40], which involves governing equations of at least 63 moments to reach satisfactory results. It will be inconvenient for practical applications due to the nontrivial solution of so many equations as well as the specification of both initial and boundary conditions for the higher-order moment variables.

In this work, we will develop a macroscopic hydrodynamic equation, together with the nonequilibrium boundary conditions, of phonon transport in a confined space rigorously for non-Fourier heat conduction at ordinary temperatures. The feature of our derivation is a perturbation expansion around the nonequilibrium distribution obtained by the maximum entropy principle, such that this macroscopic model is capable of describing both the temporal and spatial thermodynamic nonequilibrium effects in nanoscale heat transport. The remainder of this article is organized as follows: The theoretical derivation of the phonon hydrodynamic equation from the phonon Boltzmann equation is provided in Sec. II. The nonequilibrium boundary conditions of heat flux and temperature for the phonon hydrodynamic equation are developed in Sec. III. In Sec. IV, classical non-Fourier phonon heat transports including both the steady-state and transient cases are modeled to demonstrate and validate the present phonon hydrodynamic model. Concluding remarks are finally made in Sec. V.

II. PHONON HYDRODYNAMIC EQUATION

A. Phonon Boltzmann equation

The quasiparticle picture is established for phonons when heat conduction takes place in a dielectric crystal with a characteristic length much larger than the dominant phonon wavelength [41]. The transport behavior of phonons is thus described by the phonon Boltzmann equation similar to the classical Boltzmann equation for rarefied gas [42]:

$$\frac{\partial f}{\partial t} + \mathbf{v}_g \cdot \nabla_{\mathbf{x}} f = C(f), \quad (1)$$

where $f \equiv f(\mathbf{x}, t, \mathbf{k})$ is the phonon distribution function, with $f(\mathbf{x}, t, \mathbf{k}) d\mathbf{x} d\mathbf{k}$ denoting the probabilistic number of phonons found within the spatial interval $(\mathbf{x}, \mathbf{x} + d\mathbf{x})$ and wave vector interval $(\mathbf{k}, \mathbf{k} + d\mathbf{k})$ at a specific time t . The phonon group velocity \mathbf{v}_g denotes the energy propagating speed of the lattice wave and is determined from $\mathbf{v}_g = \nabla_{\mathbf{k}} \omega$ as long as the phonon dispersion relation $\omega = \omega(\mathbf{k})$ is available.

The scattering term $C(f)$ in Eq. (1) evaluates the variation of phonon distribution function due to phonon scattering processes which include mainly two categories: normal scattering (N process) and resistive scattering (R process). The energy conservation is ensured for both kinds of processes while the quasimomentum of phonons is conserved only in the N process. The full expression of the scattering term is extremely complex due to the nonlinear nature of phonon scattering processes. One common simplification is Callaway's dual

relaxation model [43], which assumes that the N process and R process restore the phonon distribution function separately to a displaced Planck distribution and a Planck distribution. Callaway's model is widely applied in studying the classical phonon hydrodynamics in low-temperature dielectric crystals [25,26,44,45], where the N process dominates over the R process. As we focus on non-Fourier heat conduction at ordinary temperatures where the N process is negligible except for the very special carbon materials [46–49], the single-mode relaxation time approximation is adopted for the phonon scattering term. In this way, the phonon Boltzmann equation becomes [1]

$$\frac{\partial f}{\partial t} + \mathbf{v}_g \cdot \nabla_{\mathbf{x}} f = -\frac{f - f_R^{\text{eq}}}{\tau_R}, \quad (2)$$

where the equilibrium distribution function for the R process is the Planck distribution:

$$f_R^{\text{eq}} = \frac{1}{\exp(\hbar\omega/k_B T) - 1}, \quad (3)$$

with $\hbar = h/2\pi$ the reduced Planck constant and k_B the Boltzmann constant.

The phonon relaxation time τ_R and phonon group velocity \mathbf{v}_g are often dependent on the phonon frequency. This kind of spectral dependency complicates the solution of Eq. (2), which usually has recourse to numerical schemes such as the discrete ordinate method (DOM) [50] and Monte Carlo (MC) method [51]. It is a difficult task to develop a unified hydrodynamic model considering the phonon spectral properties which are diverse for different materials [39,40]. To capture the common features of non-Fourier heat conduction, the following assumptions are made as a first step [3]: (i) the isotropic assumption, in which phonon properties in one crystalline direction are representative of those in the whole wave vector space; (ii) the gray assumption, in which three identical acoustic phonon branches are considered with an effective constant relaxation time, with negligible contribution from the optical phonon branches; (iii) Debye's assumption, in which the linear phonon dispersion relation $\omega = v_g k$ is adopted.

B. Balance equations of energy density and heat flux

The phonon hydrodynamic model is a macroscopic method based on field variables defined as the statistical average of the phonon distribution function:

$$e = \int \hbar\omega f d\mathbf{k}, \quad \mathbf{q} = \int \mathbf{v}_g \hbar\omega f d\mathbf{k}, \quad \mathbf{Q} = \int \mathbf{v}_g \mathbf{v}_g \hbar\omega f d\mathbf{k}, \quad (4)$$

with e , \mathbf{q} , and \mathbf{Q} denoting the phonon energy density, heat flux, and flux of heat flux, respectively. Note that the integration over wave vector space has included the summation over the three phonon branches throughout the present work. Multiplying the phonon energy quanta $\hbar\omega$ on both sides of Eq. (2) and integrating over the wave vector space, we acquire the balance equation of energy density:

$$\frac{\partial e}{\partial t} + \nabla \cdot \mathbf{q} = 0. \quad (5)$$

The right-hand side of Eq. (5) vanishes because of the energy conservation during phonon scattering. Through a similar procedure by multiplying the phonon microscopic variable $\mathbf{v}_g \hbar \omega$, we get the balance equation of the heat flux:

$$\frac{\partial \mathbf{q}}{\partial t} + \nabla \cdot \mathbf{Q} = -\frac{\mathbf{q}}{\tau_R}. \quad (6)$$

The Planck distribution has no contribution to the right-hand side of Eq. (6) since the isotropic equilibrium distribution yields no heat flux.

Equations (5) and (6) are exactly the four-moment field equations of the phonon Boltzmann equation. To have a closed description of phonon transport, the flux of heat flux \mathbf{Q} has to be specified in terms of the four basic field variables (e and the three components of \mathbf{q}), which constitutes the closure problem in kinetic theory. Two well-known methods have been established to complete the closure in classical gas kinetic theory: the Chapman-Enskog expansion method [52] and Grad's moment method [53]. The Chapman-Enskog expansion to the Boltzmann equation successfully recovers the Navier-Stokes-Fourier equations within first order whereas it gives rise to unstable hydrodynamic equations within second or higher order [52,54]. The Grad's moment method provides an approach to obtain stable higher-order hydrodynamic equations. But there are still several drawbacks to Grad's moment method, which limit its crucial applications [54]. Within about the last ten years, an approach termed the "regularized moment method" (R13 moment method) has been proposed and widely applied in modeling nonequilibrium gas flows [54–56]. The R13 moment method combines the advantages of the Chapman-Enskog expansion method and Grad's moment method, overcoming some drawbacks of each [55]. Its main idea is a Chapman-Enskog expansion around the Grad's thirteen-moment nonequilibrium distribution rather than the usual local Maxwell-Boltzmann equilibrium distribution [54,57]. As a result, the R13 equations are capable of modeling the nonequilibrium high-Knudsen-number gas flow. Inspired from the R13 moment method, we propose to accomplish the closure for phonon transport through a perturbation solution to Eq. (2) around a four-moment nonequilibrium phonon distribution obtained by the maximum entropy principle. Therefore the derived phonon hydrodynamic equation will be able to describe the strong thermodynamic nonequilibrium effects in nanoscale heat transport.

C. Four-moment nonequilibrium distribution

The maximum entropy principle is applied to derive a nonequilibrium phonon distribution dependent on the four basic field variables of phonons. The main idea of this principle is to resolve the distribution function through a maximization of entropy density under the constraints of specified field variables [25,26]. In a mathematical view, the problem reduces to maximizing the following functional:

$$\begin{aligned} \Phi = & -k_B \int [f \ln f - (1+f) \ln(1+f)] d\mathbf{k} \\ & + \beta \left(e - \int \hbar \omega f d\mathbf{k} \right) + \gamma_i \left(q_i - \int v_{gi} \hbar \omega f d\mathbf{k} \right), \quad (7) \end{aligned}$$

where the first right-hand term denotes the kinetic expression of phonon entropy density [41], β and γ_i being the Lagrange multipliers for energy density and heat flux, respectively. The extremum conditions of the functional Eq. (7) include

$$\frac{\partial \Phi}{\partial f} = \int \left[k_B \ln \left(1 + \frac{1}{f} \right) - \beta \hbar \omega - \gamma_i v_{gi} \hbar \omega \right] d\mathbf{k} = 0, \quad (8)$$

$$\frac{\partial \Phi}{\partial \beta} = e - \int \hbar \omega f d\mathbf{k} = 0, \quad (9)$$

$$\frac{\partial \Phi}{\partial \gamma_i} = q_i - \int v_{gi} \hbar \omega f d\mathbf{k} = 0. \quad (10)$$

Equations (9) and (10) represent exactly the specified energy density and heat flux, whereas Eq. (8) gives rise to the four-moment nonequilibrium distribution:

$$f_4 = \frac{1}{\exp \left(\beta \frac{\hbar \omega}{k_B} + \gamma_i \frac{v_{gi} \hbar \omega}{k_B} \right) - 1}, \quad (11)$$

where the subscript 4 in the phonon distribution function represents its dependence on the four basic field variables.

At equilibrium state, the heat flux and its corresponding Lagrange multiplier vanish, such that Eq. (11) should reduce to the Planck distribution Eq. (3). Thus the Lagrange multiplier for energy density is specified as $\beta = 1/T$. For the nonequilibrium state, Eq. (11) is further linearized when heat transport is not too far away from the equilibrium state:

$$f_4 = f_R^{\text{eq}} - \gamma_j v_{gj} T^2 \frac{\partial f_R^{\text{eq}}}{\partial T}. \quad (12)$$

The Lagrange multiplier in Eq. (12) is determined through evaluating heat flux based on the second formulation in Eq. (4):

$$q_i = -\frac{1}{3} \gamma_i T^2 \int v_g^2 \hbar \omega \frac{\partial f_R^{\text{eq}}}{\partial T} d\mathbf{k}. \quad (13)$$

Under the gray Debye assumption made in this work, Eq. (13) gives the Lagrange multiplier for heat flux as

$$\gamma_i = -\frac{3q_i}{T^2 v_g^2 C_V}. \quad (14)$$

Therefore, the four-moment nonequilibrium distribution is obtained by substituting Eq. (14) into Eq. (12):

$$f_4 = f_R^{\text{eq}} + \frac{3}{C_V v_g^2} \frac{\partial f_R^{\text{eq}}}{\partial T} q_i v_{gi}. \quad (15)$$

With the help of Eq. (15), the closure problem for the balance equation of heat flux is completed. Putting Eq. (15) into the kinetic definition of the flux of heat flux in Eq. (4), we acquire its explicit expression in terms of the energy density:

$$\mathbf{Q} = \frac{1}{3} v_g^2 e \mathbf{I}, \quad (16)$$

with \mathbf{I} denoting the unit tensor. Substituting Eq. (16) into Eq. (6), we obtain the Cattaneo-Vernotte (C-V) type heat transport equation [34]:

$$\tau_R \frac{\partial \mathbf{q}}{\partial t} + \mathbf{q} = -\lambda \nabla T. \quad (17)$$

Therefore, Eq. (17) together with Eq. (5) makes up a closed mathematical description of phonon heat transport. Below we

consider a further perturbation expansion around the four-moment nonequilibrium distribution Eq. (15). In other words, we seek a higher-order approximation to the flux of heat flux in Eq. (16). A generalized heat transport equation beyond the C-V type one will be derived.

D. Higher-order approximation

The higher-order approximation to the flux of heat flux \mathbf{Q} is derived from its balance equation, which is obtained by multiplying the phonon microscopic variable $\mathbf{v}_g \mathbf{v}_g \hbar \omega$ on both sides of Eq. (2) and integrating over the wave vector space:

$$\frac{\partial Q_{ij}}{\partial t} + \frac{\partial}{\partial x_k} M_{ijk} = \frac{1}{\tau_R} \left(\frac{1}{3} v_g^2 e \delta_{ij} - Q_{ij} \right), \quad (18)$$

with the flux of \mathbf{Q} being a third-order tensor and defined as

$$M_{ijk} = \int v_{gi} v_{gj} v_{gk} \hbar \omega f d\mathbf{k}. \quad (19)$$

Before a regular perturbation expansion, Eq. (18) is rescaled as

$$\frac{\partial Q_{ij}}{\partial t} + \frac{\partial}{\partial x_k} M_{ijk} = \frac{1}{\varepsilon \tau_R} \left(\frac{1}{3} v_g^2 e \delta_{ij} - Q_{ij} \right). \quad (20)$$

The theoretical foundation for the scaling in Eq. (20) comes from the scaling of the phonon Boltzmann Eq. (2), which can be nondimensionalized into the following form [58]:

$$\text{Sr} \frac{\partial f^*}{\partial t^*} + \mathbf{v}_g^* \cdot \nabla_{\mathbf{x}^*} f^* = \frac{C(f^*)}{\text{Kn}}, \quad (21)$$

where all the variables with the ‘‘star’’ superscript denote the dimensionless variables, with Sr and Kn the Strouhal number and Knudsen number, respectively [58]. In the classical Chapman-Enskog expansion to the Boltzmann equation, the hydrodynamic equations are derived in the limit of a very small Knudsen number ($\text{Kn} < 0.01$). For the transport process with strong nonequilibrium effects considered in the present work, the Knudsen number could be finite. Nevertheless, the development of the phonon hydrodynamics is restricted to the situation where the Knudsen number is smaller than 0.3 as will be shown later. Therefore, the Knudsen number can still be approximated as a small parameter, and is adopted for the ε in Eq. (20). Two Knudsen numbers will be introduced in this work: the spatial Knudsen number defined as the ratio of phonon mean-free path to the characteristic length, and the temporal Knudsen number defined as the ratio of phonon relaxation time to the characteristic time. A similar approximation was also made in the regularized moment method for high-Knudsen-number gas flow [55], where the small parameter ε is used to represent the order of magnitude of each term and will be set to unity at the end of the perturbation expansion:

$$Q_{ij} = Q_{ij}^{(0)} + \varepsilon Q_{ij}^{(1)} + \dots \quad (22)$$

Substituting Eq. (22) into Eq. (20), we obtain terms at each order of magnitude on the small parameter respectively:

$$\varepsilon^{-1} : Q_{ij}^{(0)} = \frac{1}{3} v_g^2 e \delta_{ij}, \quad (23)$$

$$\varepsilon^0 : \left[\frac{\partial Q_{ij}^{(0)}}{\partial t} + \frac{\partial}{\partial x_k} M_{ijk}^{(0)} \right] \Big|_{f_4} = -\frac{1}{\tau_R} Q_{ij}^{(1)}. \quad (24)$$

The zeroth-order approximation of Q_{ij} in Eq. (23) is exactly Eq. (16) corresponding to the phonon distribution function f_4 in Eq. (15). The first-order approximation of Q_{ij} is related to its zeroth-order approximation from Eq. (24):

$$Q_{ij}^{(1)} = -\tau_R \left[\frac{\partial}{\partial t} (Q_{ij}^{(0)}|_{f_4}) + \frac{\partial}{\partial x_k} (M_{ijk}^{(0)}|_{f_4}) \right], \quad (25)$$

where the zeroth-order approximations for \mathbf{Q} and the flux of \mathbf{Q} are evaluated at the phonon distribution function f_4 as

$$Q_{ij}^{(0)}|_{f_4} = \frac{1}{3} v_g^2 e \delta_{ij}, \quad M_{ijk}^{(0)}|_{f_4} = \frac{1}{5} v_g^2 (\delta_{ij} q_k + \delta_{ik} q_j + \delta_{jk} q_i). \quad (26)$$

Therefore the first-order approximation of Q_{ij} is acquired by substituting Eq. (26) into Eq. (25):

$$Q_{ij}^{(1)} = \frac{2}{15} \tau_R v_g^2 \frac{\partial q_k}{\partial x_k} \delta_{ij} - \frac{1}{5} \tau_R v_g^2 \left(\frac{\partial q_i}{\partial x_j} + \frac{\partial q_j}{\partial x_i} \right). \quad (27)$$

Combining the zeroth-order approximation Eq. (23) and first-order approximation Eq. (27), we get the explicit expression for the flux of heat flux \mathbf{Q} :

$$Q_{ij} = \frac{1}{3} v_g^2 e \delta_{ij} + \frac{2}{15} \tau_R v_g^2 \frac{\partial q_k}{\partial x_k} \delta_{ij} - \frac{1}{5} \tau_R v_g^2 \left(\frac{\partial q_i}{\partial x_j} + \frac{\partial q_j}{\partial x_i} \right). \quad (28)$$

Higher-order approximate terms for the flux of heat flux are thus derived in the form of the gradient of heat flux, which is crucial for modeling nanoscale heat transport. Actually, such terms have been called the *nonlocal terms* to describe the size effect in several previous phenomenological macroscopic heat transport models [19,20,59]. However, a rigorous derivation of them from the phonon Boltzmann equation has been seldom reported. This work aims to remedy this gap by providing a theoretical ground for the nonlocal terms in macroscopic models.

The phonon hydrodynamic equation is achieved by substituting the flux of heat flux Eq. (28) into the balance equation of heat flux Eq. (6):

$$\tau_R \frac{\partial \mathbf{q}}{\partial t} + \mathbf{q} = -\lambda \nabla T + \frac{1}{5} \Lambda^2 \left[\nabla^2 \mathbf{q} + \frac{1}{3} \nabla (\nabla \cdot \mathbf{q}) \right]. \quad (29)$$

The average mean-free path in Eq. (29) is fully expressed as $\Lambda = v_g \tau_R$. Since it uses the same field variables as the traditional Fourier’s description, the present hydrodynamic model avoids the complexity of classical moment methods involving the governing equation of higher-order moments [25,26,40]. Comparing to the C-V type heat transport Eq. (17), Eq. (29) contains also nonlocal terms of heat flux, which are the key ingredients to capture the spatial nonequilibrium effects in extremely small heat conduction. In comparison to

the Fourier's law, the other relaxation term of heat flux in Eq. (29) aims at capturing the temporal nonequilibrium effects in ultrafast heat conduction. In the diffusive limit where both relaxation and nonlocal effects are negligible, Eq. (29) reduces exactly to the Fourier's law.

The preceding derivation of Eq. (29) at the level of the moment equations has a counterpart in view of the phonon distribution function. The perturbation expansion around f_4 gives rise to the phonon distribution function as

$$f = f_R^{\text{eq}} - \tau_R \left(\frac{\partial f}{\partial t} + \mathbf{v}_g \cdot \nabla f \right) \Big|_{f_4}. \quad (30)$$

Substituting Eq. (15) into Eq. (30), we obtain the expression of the phonon distribution function:

$$f = f_R^{\text{eq}} + \frac{3}{C_V v_g^2} \frac{\partial f_R^{\text{eq}}}{\partial T} q_i v_{gi} + \frac{\tau_R}{C_V} \frac{\partial q_i}{\partial x_i} \frac{\partial f_R^{\text{eq}}}{\partial T} - \frac{3\tau_R}{C_V v_g^2} v_{gi} v_{gj} \frac{\partial q_i}{\partial x_j} \frac{\partial f_R^{\text{eq}}}{\partial T}. \quad (31)$$

Equation (31) is exactly the nonequilibrium phonon distribution function corresponding to the phonon hydrodynamic equation (29). It can be checked that Eq. (31) recovers precisely the energy density e , the heat flux \mathbf{q} , and the flux of heat flux Eq. (28), respectively. Furthermore, the derived nonequilibrium phonon distribution Eq. (31) is dependent on the field variables and their gradients, in a different way from that as a function of local field variables in the classical Grad's type moment method [25,26,40,44]. In contrast to the second- or higher-order Chapman-Enskog expansion solution with higher-order gradient terms of field variables as a source of instability [52], the present closure method yields a nonequilibrium phonon distribution involving only first-order gradient terms ensuring a stable hydrodynamic equation.

Finally, a comparison is made between the phonon hydrodynamic equation (29) and classical phonon hydrodynamic equations in low-temperature dielectric crystals. The G-K equation obtained with the eigenvalue analysis method is [23,24]

$$\tau_R \frac{\partial \mathbf{q}}{\partial t} + \mathbf{q} = -\lambda \nabla T + \frac{1}{5} v_g^2 \tau_N \tau_R [\nabla^2 \mathbf{q} + 2\nabla(\nabla \cdot \mathbf{q})]. \quad (32)$$

A phonon hydrodynamic equation with one slightly different coefficient in nonlocal terms of heat flux was derived through the maximum entropy moment method in the limit of small relaxation time of the N process (τ_N) [25,26]:

$$\tau_R \frac{\partial \mathbf{q}}{\partial t} + \mathbf{q} = -\lambda \nabla T + \frac{1}{5} v_g^2 \tau_N \tau_R \left[\nabla^2 \mathbf{q} + \frac{1}{3} \nabla(\nabla \cdot \mathbf{q}) \right]. \quad (33)$$

The tiny coefficient difference between Eq. (32) and Eq. (33) has been explained in the framework of Chapman-Enskog expansion in our recent work [3]. Although the two equations have a similar mathematical form to Eq. (29), the underlying heat transport mechanisms are very different. The nonlocal terms of heat flux in the classical phonon hydrodynamic equations (32) and (33) originates from the nonresistive phonon normal scattering. They represent the transfer of phonon quasimomentum through the momentum-conserving normal scattering, with the same physical meaning as the viscous term in the Navier-Stokes equation for gas

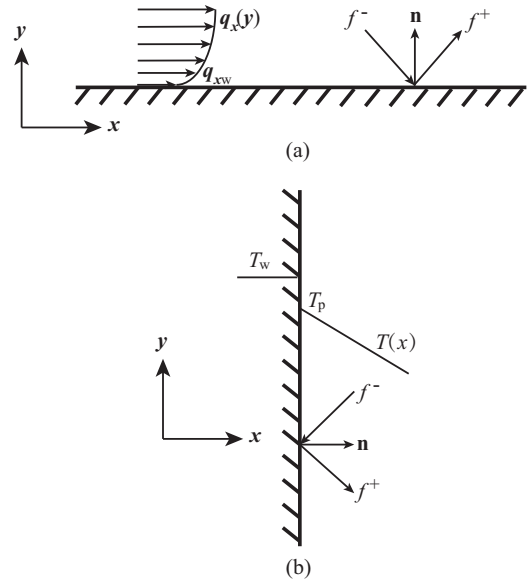


FIG. 1. Derivation of nonequilibrium boundary conditions for the phonon hydrodynamic equation: (a) heat flux tangential retardant (HFTR) boundary condition; (b) temperature jump boundary condition. The solid lines represent the heat flux and temperature profiles. f^- and f^+ represent the distribution functions of incident phonons and reflecting phonons, respectively.

flow. In contrast, the nonlocal terms of heat flux in the present phonon hydrodynamic equation (29) are representative of the spatial nonequilibrium effects from phonon-boundary scattering or large spatial thermal variation. As a result, the G-K heat transport equation is usually suitable for heat transport in bulk dielectric crystals in low-temperature situations [23–26,60,61], while the present phonon hydrodynamic equation (29) is developed for nanoscale heat transport at ordinary temperatures. To have a complete mathematical description, the nonequilibrium boundary conditions of heat flux and temperature are developed for the phonon hydrodynamic equation in the following section.

III. NONEQUILIBRIUM BOUNDARY CONDITIONS

In non-Fourier heat conduction at ordinary temperature, there are mainly two macroscopic manifestations from thermodynamic nonequilibrium effects: (i) the reduction of tangential heat flux near an adiabatic surface due to enhanced phonon-boundary scattering, as shown in Fig. 1(a); (ii) the noncontinuous temperature distribution near an isothermal surface due to insufficient phonon-boundary interaction and thermalization, as shown in Fig. 1(b). The temperature jump and velocity slip boundary conditions have been fully established to describe the noncontinuous temperature and velocity distributions in high-Knudsen-number gas flows [62]. A phenomenological heat flux slip boundary condition was directly borrowed from the gas velocity slip boundary condition [19,63]. However, the gas flow and phonon flow are quite different; for instance, the gas velocity vanishes at the wall (“non-slip”) in the continuum regime wherein the phonon heat flux remains a finite value (“finite-slip” or “infinite-slip”) as predicted by

the Fourier's law [3]. The tangential heat flux reduces near the adiabatic boundary as the surface imposes retardancy on the phonon flow. Thus we propose a heat flux tangential retardant (HFTR) boundary condition for phonon flow in confined space. The essential difference between the HFTR boundary condition and velocity slip boundary condition will be further elucidated through the case of in-plane transport in Sec. IV A 1. On the other hand, the terminology "temperature jump boundary condition" is still used since the temperature jump in phonon flow holds almost the same physical picture as that in high-Knudsen-number gas flow. Both the HFTR and temperature jump boundary conditions are developed for the phonon hydrodynamic equation in this section.

Our derivation is based on the principle in classical kinetic theory [53,64] in which the boundary condition for a specific macroscopic field variable (the corresponding microscopic variable ϕ) is derived through the balance equation of its flux at the boundary [64]:

$$\int_{\Omega} f \phi \mathbf{v}_g d\mathbf{k} = \int_{\Omega^-} f^- \phi \mathbf{v}_g d\mathbf{k} + \int_{\Omega^+} f^+ \phi \mathbf{v}_g d\mathbf{k}, \quad (34)$$

with Ω , Ω^- , Ω^+ denoting the whole wave vector space, the hemispherical wave vector space with $\mathbf{k} \cdot \mathbf{n} < 0$, and the hemispherical wave vector space with $\mathbf{k} \cdot \mathbf{n} > 0$, respectively. \mathbf{n} is the surface unit normal vector as shown in Fig. 1. As long as the expressions of the distribution function of incident phonons (f^-) and reflecting phonons (f^+) are known, Eq. (34) relates the field variables of phonons near the surface to those at the surface, exactly the boundary conditions. The distribution function of incident phonons is available from the nonequilibrium solution Eq. (31) in Sec. IID. The distribution function of reflecting phonons is related to that of incident phonons through the phonon-surface interaction model. The most common Maxwell model is adopted here [65]:

$$f^+(\mathbf{x}, t, \mathbf{k}) = s f^-(\mathbf{x}, t, \mathbf{k}') + (1-s) f_R^{\text{eq}}(\mathbf{x}, t, \mathbf{k}), \quad (35)$$

where $\mathbf{k}' \equiv \mathbf{k} - 2(\mathbf{n} \cdot \mathbf{k})\mathbf{n}$ denotes the wave vector of phonons experiencing specular scattering, and s is the specular parameter, with s and $1-s$ denoting the portion of phonons experiencing specular scattering and diffuse scattering, respectively. The thermalizing diffuse scattering is considered in Eq. (35) which assumes that the incident phonons leave the boundary after reaching thermal equilibrium with the surface. Although the nonthermalizing diffuse scattering is discussed in some recent literature [26,66], we choose the thermalizing one due to both its simple formulation and wide applications in Boltzmann equation modeling of phonon heat transport [1,16,67,68]. In addition, later we will show that the difference between mesoscopic diffuse scattering schemes is smoothed out after an upgrade of the level of description to macroscopic one. The present macroscopic model can still produce consistent results with the Monte Carlo simulation using the nonthermalizing diffuse scheme for heat conduction through thin films with adiabatic lateral surfaces.

A. Heat flux tangential retardant boundary condition

To derive the boundary condition for heat flux, the phonon microscopic variable $\phi = \mathbf{v}_g \hbar \omega$ is put into Eq. (34). As shown in Fig. 1(a), we consider a steady-state phonon transport paral-

lel to an adiabatic surface under a uniform temperature gradient such that the heat flux depends merely on the coordinate y . In this case, Eq. (34) reduces to

$$\begin{aligned} & \int_{\Omega} f \hbar \omega v_{gx} v_{gy} d\mathbf{k} \\ &= \int_{\Omega^-} f^- \hbar \omega v_{gx} v_{gy} d\mathbf{k} + \int_{\Omega^+} f^+ \hbar \omega v_{gx} v_{gy} d\mathbf{k}. \end{aligned} \quad (36)$$

The distribution function of phonons incident on the surface is obtained from Eq. (31):

$$f^- = f_R^{\text{eq}} + \frac{3}{C_V v_g^2} \frac{\partial f_R^{\text{eq}}}{\partial T} q_{xw} v_{gx} - \frac{3\tau_R}{C_V v_g^2} v_{gx} v_{gy} \left(\frac{\partial q_x}{\partial y} \right)_w \frac{\partial f_R^{\text{eq}}}{\partial T}. \quad (37)$$

The distribution function of phonons leaving the surface is determined from Eq. (35):

$$f^+ = s f^-(v_{gx}, -v_{gy}) + (1-s) f_R^{\text{eq}}. \quad (38)$$

The first term on the right-hand side of Eq. (36) is resolved by substituting Eq. (37) inside and integrating over the hemispherical wave vector space:

$$\int_{\Omega^-} f^- \hbar \omega v_{gx} v_{gy} d\mathbf{k} = -\frac{3}{16} v_g q_{xw} - \frac{1}{10} \tau_R v_g^2 \left(\frac{\partial q_x}{\partial y} \right)_w. \quad (39)$$

The second term on the right-hand side of Eq. (36) is resolved by substituting Eq. (37) and Eq. (38) inside and then integrating over the hemispherical wave vector space:

$$\int_{\Omega^+} f^+ \hbar \omega v_{gx} v_{gy} d\mathbf{k} = s \left[\frac{3}{16} v_g q_{xw} + \frac{1}{10} \tau_R v_g^2 \left(\frac{\partial q_x}{\partial y} \right)_w \right]. \quad (40)$$

Putting Eq. (39) and Eq. (40) into Eq. (36), we acquire the following relation at the boundary:

$$Q_{xy} = (s-1) \left[\frac{3}{16} v_g q_{xw} + \frac{1}{10} \tau_R v_g^2 \left(\frac{\partial q_x}{\partial y} \right)_w \right]. \quad (41)$$

One also has the constitutive relation for the flux of heat flux at the boundary from Eq. (28):

$$Q_{xy} = -\frac{1}{5} \tau_R v_g^2 \left(\frac{\partial q_x}{\partial y} \right)_w. \quad (42)$$

A combination of Eq. (41) and Eq. (42) results in the HFTR boundary condition:

$$q_{xw} = \frac{1+s}{1-s} \frac{8}{15} \Lambda \left(\frac{\partial q_x}{\partial y} \right)_w. \quad (43)$$

It is seen that the surface heat flux is proportional to the gradient of heat flux near the surface. For the special case of a fully diffuse surface often considered in engineering ($s=0$), Eq. (43) reduces to

$$q_{xw} = \frac{8}{15} \Lambda \left(\frac{\partial q_x}{\partial y} \right)_w. \quad (44)$$

The present derivation based on a straight surface can be extended for curved surfaces, where Eq. (43) is generalized

to

$$\mathbf{q}_w = \frac{1+s}{1-s} \frac{8}{15} \Lambda \nabla_{\mathbf{n}} \mathbf{q}, \quad (45)$$

with $\nabla_{\mathbf{n}}$ denoting the local gradient along the surface normal direction.

B. Temperature jump boundary condition

To derive the boundary condition for temperature (energy density), the phonon microscopic variable $\phi = \hbar\omega$ is substituted into Eq. (34). As shown in Fig. 1(b), a one-dimensional (1D) steady-state phonon transport normal to an isothermal surface is considered. In this case, Eq. (34) reduces to

$$\int_{\Omega} f \hbar\omega v_{gx} d\mathbf{k} = \int_{\Omega^-} f^- \hbar\omega v_{gx} d\mathbf{k} + \int_{\Omega^+} f^+ \hbar\omega v_{gx} d\mathbf{k}. \quad (46)$$

Based on the energy conservation principle, one has vanishing divergence of heat flux: $\partial q_x / \partial x = 0$. Therefore, the distribution function of phonons incident on the surface is reduced from Eq. (31) as

$$f^- = f_{\text{R}}^{\text{eq}}(T_p) + \frac{3}{C_V v_g^2} \frac{\partial f_{\text{R}}^{\text{eq}}}{\partial T} q_x v_{gx}, \quad (47)$$

with T_p denoting the temperature of phonons in the vicinity of the surface. The distribution function of phonons leaving the surface is specified from Eq. (35) as

$$f^+ = s f^-(-v_{gx}, v_{gy}) + (1-s) f_{\text{R}}^{\text{eq}}(T_w), \quad (48)$$

with T_w denoting the temperature of the heat source. The first term on the right-hand side of Eq. (46) is resolved by putting Eq. (47) inside and integrating over the hemispherical wave vector space:

$$\int_{\Omega^-} f^- \hbar\omega v_{gx} d\mathbf{k} = -\frac{1}{4} v_g e(T_p) + \frac{1}{2} q_x. \quad (49)$$

The second term on the right-hand side of Eq. (46) is resolved by substituting Eq. (47) and Eq. (48) inside and then integrating over the hemispherical wave vector space:

$$\int_{\Omega^+} f^+ \hbar\omega v_{gx} d\mathbf{k} = s \left[\frac{1}{4} v_g e(T_p) - \frac{1}{2} q_x \right] + (1-s) \frac{1}{4} v_g e(T_w). \quad (50)$$

In deriving Eq. (49) and Eq. (50), the following correlation has been used:

$$\int_{\Omega^+} f_{\text{R}}^{\text{eq}} \hbar\omega v_{gx} d\mathbf{k} = - \int_{\Omega^-} f_{\text{R}}^{\text{eq}} \hbar\omega v_{gx} d\mathbf{k} = \frac{1}{4} v_g e, \quad (51)$$

which can be obtained through the following relations after partial integration over the solid angle:

$$\int_{\Omega^+} f_{\text{R}}^{\text{eq}} \hbar\omega v_{gx} d\mathbf{k} = \frac{3}{(2\pi)^3} \pi \int_0^{k_{\text{D}}} \frac{\hbar v_g^2 k^3}{\exp(\hbar\omega/k_{\text{B}}T) - 1} dk, \quad (52)$$

$$e = \int_{\Omega} f_{\text{R}}^{\text{eq}} \hbar\omega d\mathbf{k} = \frac{3}{(2\pi)^3} 4\pi \int_0^{k_{\text{D}}} \frac{\hbar v_g k^3}{\exp(\hbar\omega/k_{\text{B}}T) - 1} dk. \quad (53)$$

The upper limit of the wave number in Eq. (52) and Eq. (53) is related to the Debye frequency (ω_{D}) as $k_{\text{D}} = \omega_{\text{D}}/v_g$. The coefficients 3 and 2π come from the number of acoustic phonon branches and the elemental volume in wave vector space, respectively. Putting Eq. (49) and Eq. (50) into Eq. (46), we acquire the following relation at the boundary:

$$q_x = \frac{1-s}{1+s} \frac{1}{2} v_g C_V (T_w - T_p), \quad (54)$$

where $e(T_w) - e(T_p) \cong C_V (T_w - T_p)$ has been assumed within first-order Taylor expansion when the heat transport is driven under a relatively small temperature difference. One also has the constitutive relation for the heat flux at the boundary from Eq. (29):

$$q_x = -\lambda \frac{dT}{dx} = -\frac{1}{3} C_V v_g^2 \tau_{\text{R}} \frac{dT}{dx}. \quad (55)$$

The combination of Eq. (54) and Eq. (55) gives rise to the temperature jump boundary condition as

$$T_w - T_p \cong -\frac{1+s}{1-s} \frac{2}{3} \Lambda \frac{dT}{dx}. \quad (56)$$

It is seen that the temperature jump at an isothermal surface is proportional to the temperature gradient near the surface. For the special case of a fully diffuse heat source (phonon black-body) often considered in engineering applications ($s = 0$), Eq. (56) reduces to

$$T_w - T_p \cong -\frac{2}{3} \Lambda \frac{dT}{dx}. \quad (57)$$

The temperature jump boundary condition Eq. (57) for the fully diffuse case has been obtained in a recent work through an approximate solution to the one-dimensional steady-state phonon Boltzmann equation [69]. Nevertheless, the present result Eq. (56) is more general than the previous one Eq. (57). Furthermore, we provide a consistent framework for developing the boundary conditions for both heat flux and temperature.

IV. RESULTS AND DISCUSSION

In this section, the phonon hydrodynamic model developed in Sec. II and Sec. III is extensively validated with both steady-state and transient nanoscale heat transport at room temperature. Steady-state cases will be investigated in Sec. IV A including in-plane and cross-plane phonon transport through thin film and phonon transport through nanowire. Transient cases are investigated in Sec. IV B including the 1D transient phonon transport across thin films, the high-frequency periodic heating of a semi-infinite surface in a frequency domain thermoreflectance (FDTR) experiment [70,71], and the heat conduction in a transient thermal grating (TTG) experiment [16,72] for the measurement of thermal properties of nanostructures. The analytical solutions of the phonon hydrodynamic model are obtained and compared to the solutions of the phonon Boltzmann equation or experimental results.

A. Steady-state nanoscale heat transport

1. In-plane phonon transport through a thin film

For the in-plane phonon transport shown in Fig. 2(a), a uniform temperature gradient $-dT/dx$ is exerted along the thin film with an arbitrary surface specularity parameter s from

0 (fully diffuse) to 1 (fully specular). The Fuchs-Sondheimer model originally proposed for in-plane electron transport has been extended to in-plane phonon transport [1]. In this model, the analytical solution of the steady-state phonon Boltzmann equation with the Maxwell boundary condition Eq. (35) is obtained as [16,67]

$$g(y, \theta, \varphi) = \begin{cases} \tau_R v_g \sin \theta \cos \varphi \frac{\partial f_R^{eq}}{\partial T} \frac{dT}{dx} \left[\frac{(1-s) \exp\left(-\frac{y}{\Lambda \cos \theta}\right)}{1-s \exp\left(-\frac{d}{\Lambda \cos \theta}\right)} - 1 \right], & 0 \leq \theta \leq \frac{\pi}{2}, \\ \tau_R v_g \sin \theta \cos \varphi \frac{\partial f_R^{eq}}{\partial T} \frac{dT}{dx} \left[\frac{(1-s) \exp\left(-\frac{y-d}{\Lambda \cos \theta}\right)}{1-s \exp\left(\frac{d}{\Lambda \cos \theta}\right)} - 1 \right], & \frac{\pi}{2} \leq \theta \leq \pi, \end{cases} \quad (58)$$

where the deviation of the phonon distribution function from the equilibrium distribution is introduced as $g = f - f_R^{eq}$. θ and φ denote the zenith angle and azimuthal angle, respectively, for characterizing the direction of phonon motion as shown in Fig. 2. The heat flux distribution is obtained by substituting Eq. (58) into the second formulation in Eq. (4):

$$q^*(Y) = \frac{3}{4} \int_0^1 (1 - \mu^2) \left\{ 2 - \frac{(1-s) [\exp(-\frac{Y}{\mu Kn_l}) + \exp(\frac{Y-1}{\mu Kn_l})]}{1-s \exp(-\frac{1}{\mu Kn_l})} \right\} d\mu, \quad (59)$$

where the directional cosine is $\mu \equiv \cos \theta$ and the dimensionless coordinate and heat flux are defined respectively as $Y \equiv y/d$ and $q^*(Y) \equiv \frac{q_x(y)}{-\lambda dT/dx}$. The spatial Knudsen number is defined as the ratio of the phonon mean-free path to the thin-film thickness: $Kn_l \equiv \Lambda/d$. The effective in-plane thermal conductivity of the thin film is acquired through an integration of the local heat flux along the cross section:

$$\frac{\lambda_{eff}}{\lambda_b} = \int_0^1 q^*(Y) dY, \quad (60)$$

where $\lambda_b = \lambda$ is the bulk thermal conductivity. Substitution of Eq. (59) into Eq. (60) results in the effective in-plane thermal conductivity of the thin film [1]:

$$\frac{\lambda_{eff}}{\lambda_b} = 1 - \frac{3(1-s)}{2\xi} \int_0^1 \mu(1 - \mu^2) \frac{1 - \exp(-\xi/\mu)}{1-s \exp(-\xi/\mu)} d\mu, \quad (61)$$

where $\xi = 1/Kn_l$ is the inverse of the spatial Knudsen number.

The in-plane phonon transport through the thin film is also modeled by the phonon hydrodynamic equation (29), which reduces to

$$q_x = -\lambda \frac{dT}{dx} + \frac{1}{5} \Lambda^2 \frac{d^2 q_x}{dy^2}. \quad (62)$$

The boundary conditions for this second-order ordinary differential equation of heat flux include the HFTR boundary in Sec. III A and the symmetrical boundary along the center line of the thin film:

$$y = 0, \quad q_x = \frac{1+s}{1-s} \frac{8}{15} \Lambda \left(\frac{dq_x}{dy} \right)_w, \quad y = \frac{d}{2}, \quad \frac{dq_x}{dy} = 0. \quad (63)$$

The heat flux distribution is resolved through a solution of Eq. (62) with the help of boundary conditions Eq. (63):

$$q^*(Y) = 1 + \frac{\exp\left[\frac{\sqrt{5}}{Kn_l} \left(Y - \frac{1}{2}\right)\right] + \exp\left[-\frac{\sqrt{5}}{Kn_l} \left(Y - \frac{1}{2}\right)\right]}{\left(\frac{1+s}{1-s} \frac{8}{3\sqrt{5}} - 1\right) \exp\left(-\frac{\sqrt{5}}{2Kn_l}\right) - \left(\frac{1+s}{1-s} \frac{8}{3\sqrt{5}} + 1\right) \exp\left(\frac{\sqrt{5}}{2Kn_l}\right)}, \quad (64)$$

where the dimensionless variables and parameters are the same as those in Eq. (59). The effective in-plane thermal conductivity of the thin film is achieved by putting Eq. (64) into Eq. (60):

$$\frac{\lambda_{eff}}{\lambda_b} = 1 + \frac{\frac{2Kn_l}{\sqrt{5}} \left[\exp\left(\frac{\sqrt{5}}{2Kn_l}\right) - \exp\left(-\frac{\sqrt{5}}{2Kn_l}\right) \right]}{\left(\frac{1+s}{1-s} \frac{8}{3\sqrt{5}} - 1\right) \exp\left(-\frac{\sqrt{5}}{2Kn_l}\right) - \left(\frac{1+s}{1-s} \frac{8}{3\sqrt{5}} + 1\right) \exp\left(\frac{\sqrt{5}}{2Kn_l}\right)}. \quad (65)$$

The comparison of cross-sectional heat flux distributions for in-plane phonon transport is shown in Fig. 3, where an overall good agreement is achieved between the present hydrodynamic modeling results and the Boltzmann equation

solutions. With increasing Kn_l , the heat flux distribution across the thin film becomes more nonuniform as a result of the spatial thermodynamic nonequilibrium effect. The heat flux near the surface is reduced from the confinement of phonon-

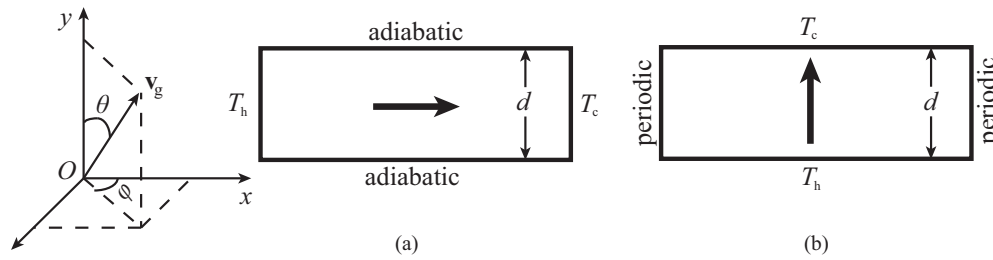


FIG. 2. Schematic of phonon transport through a thin film with a thickness d : (a) in-plane transport; (b) cross-plane transport. T_h and T_c are the temperatures of hot and cold sources, respectively.

boundary scattering, which is enhanced relative to the intrinsic phonon-phonon scattering at a smaller thin-film thickness. The phonon hydrodynamic model captures this non-Fourier feature

through both the nonlocal term of heat flux in the heat transport equation and the HFTR boundary condition. Therefore, the predicted effective in-plane thermal conductivity of the thin

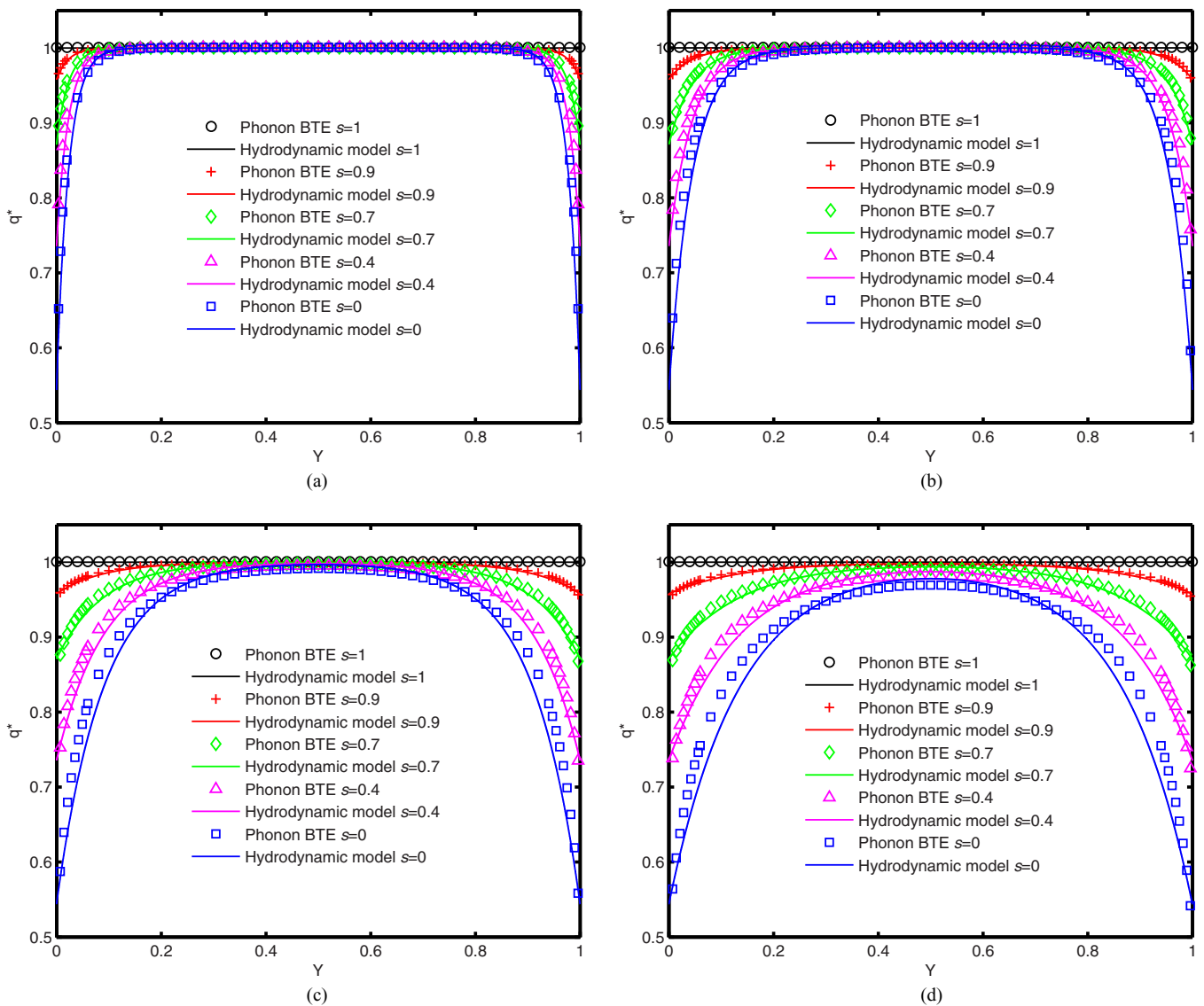


FIG. 3. The dimensionless cross-sectional heat flux distributions for in-plane phonon transport through thin film at different spatial Knudsen numbers: (a) $Kn_l = 0.05$, (b) $Kn_l = 0.1$, (c) $Kn_l = 0.2$, (d) $Kn_l = 0.3$. The solid lines represent the analytical solution Eq. (64) based on the present phonon hydrodynamic model, whereas the symbols represent the analytical solution Eq. (59) (Fuchs-Sondheimer model) based on the phonon Boltzmann transport equation (BTE). Different specularities parameters are considered for the lateral surface of the thin film: $s = 1$ (circle), $s = 0.9$ (plus), $s = 0.7$ (diamond), $s = 0.4$ (triangle), $s = 0$ (square). The spatial Knudsen number is defined as the ratio of phonon mean-free path to the thin-film thickness: $Kn_l \equiv \Lambda/d$.

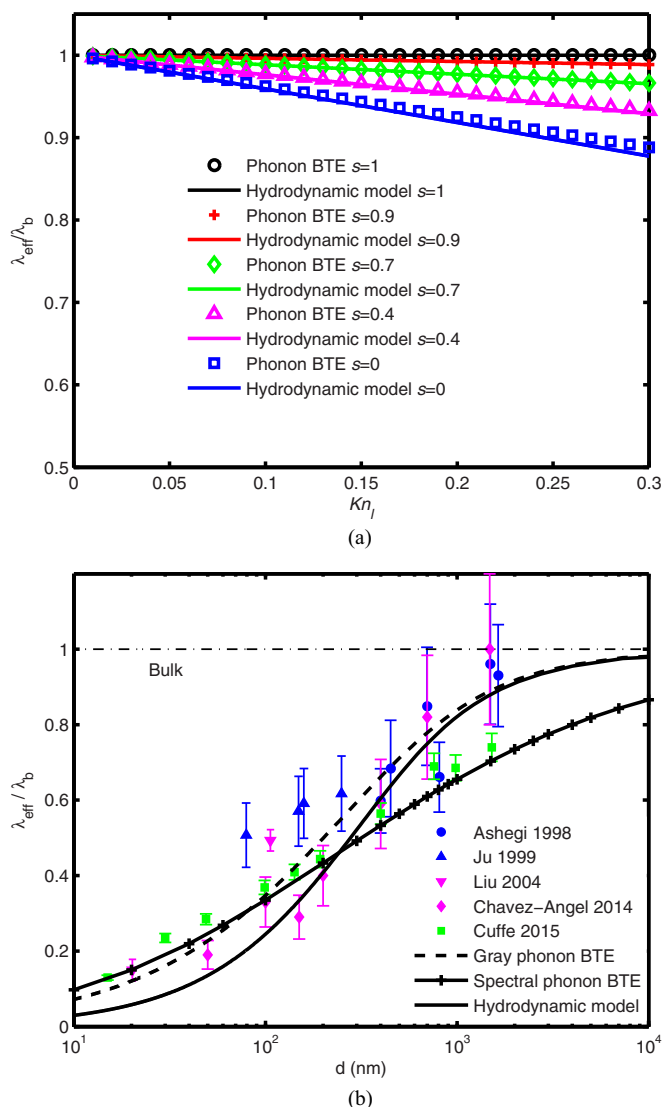


FIG. 4. The dimensionless effective in-plane thermal conductivity of the thin film. (a) Comparison to the theoretical solution. The solid lines represent the analytical solution Eq. (65) based on the present phonon hydrodynamic model, whereas the symbols represent the analytical solution Eq. (61) (Fuchs-Sondheimer model) based on the phonon Boltzmann transport equation (BTE). Different specularities parameters are considered for the lateral surface of the thin film: $s = 1$ (circle), $s = 0.9$ (plus), $s = 0.7$ (diamond), $s = 0.4$ (triangle), $s = 0$ (square). The spatial Knudsen number is defined as the ratio of phonon mean-free path to the thin-film thickness: $Kn_l \equiv \Lambda/d$. (b) Comparison to experimental results of thin films with a diffuse lateral surface ($s = 0$) at room temperature ($T = 300$ K). The symbols with error bars are experimental data from the literature [16,73–76], whereas the dashed line and solid line represent respectively the solutions of the gray phonon BTE [16] and the present phonon hydrodynamic model with a median-thermal-conductivity phonon mean-free path $\Lambda_m = 441$ nm [72,77]. The solid line with the cross symbol denotes the solution of the spectral phonon BTE [16].

film agrees well with the Fuchs-Sondheimer model, as shown in Fig. 4(a). It is also seen that the spatial nonequilibrium effect decreases with increasing value of the specularities parameter, which can be explained by a larger effective thin-film thickness

for a smoother surface. In all, the phonon hydrodynamic model gives appreciably accurate results at a spatial Knudsen number smaller than about 0.3, i.e., up to the slip regime and early transition regime. The result of the phonon hydrodynamic model is further compared to the experimental measurement of thermal conductivity of silicon thin films at room temperature [16,73–76], as shown in Fig. 4(b), where a global agreement is acquired. A fully diffuse scheme is used for phonon-boundary scattering at the thin film surface [16,67]. The phonon spectral property is taken into account by introducing an effective “median-thermal-conductivity MFP,” Λ_m , which is defined as the MFP of phonons larger than Λ_m contributing to 50% of the bulk thermal conductivity from the phonon MFP spectra [72,77]. The phonon MFP spectra of silicon at room temperature have been reconstructed by different experimental or computational methods, which produce a range of values for Λ_m . The results by the *ab initio* method ($\Lambda_m = 547$ nm) and the molecular dynamics simulation ($\Lambda_m = 335$ nm) have been recommended as the most two accurate ones [77]. Therefore, we adopt the value of median-thermal-conductivity MFP of phonons $\Lambda_m = 441$ nm as an average of the two results. The adopted value of the median-thermal-conductivity MFP is also consistent with that ($\sim 0.5 \mu\text{m}$) in Ref. [72], where Λ_m has been suggested as a more useful parameter in analyzing the onset of size effects in thermal conductivity.

Through the present study, some essential differences are inferred between the nonequilibrium effects and hydrodynamic modeling in micro/nanoscale gas flow and phonon flow. As is known the Fourier’s law and Navier-Stokes equation describe well the behaviors of heat and fluid flow in the continuum regime. For gas flow in the slip regime and early transition regime, the Navier-Stokes equation can still provide an appreciably good prediction of the velocity profile when supplemented with velocity slip boundary conditions including first-order and second-order ones [62], as shown in Fig. 5(a). In comparison, once phonon heat transport deviates from the continuum (diffusive) regime, the Fourier’s law no longer works in capturing any tiny amount of reduction of heat flux near an adiabatic surface. The correction of the constitutive heat transport equation is crucial for an adequate description of phonon flow in a confined space. In other words, the nonlocal terms of heat flux in Eq. (29) are indispensable for modeling phonon transport in the slip regime and early transition regime as shown in Fig. 5(b). This difference in hydrodynamic modeling originates from the underlying different microscopic dynamics of gas molecules and phonons. Gas molecules obey the classical Maxwell-Boltzmann statistics and the total momentum is conserved during molecule-molecule scattering [52]. In the gas Poiseuille flow shown in Fig. 5(a), the momentum transfers from the internal molecules to the molecules near the wall and is finally destroyed by the wall. Therefore, a vanishing macroscopic gas velocity at the wall is observed in the continuum regime, where the Navier-Stokes equation with the non-slip velocity boundary condition works well [62]. Phonons are instead bosons obeying the quantum Bose-Einstein statistics with the total momentum not conserved during phonon-phonon umklapp scattering at ordinary temperature [1,41]. In the phonon flow shown in Fig. 5(b), the umklapp scattering taking place everywhere tends

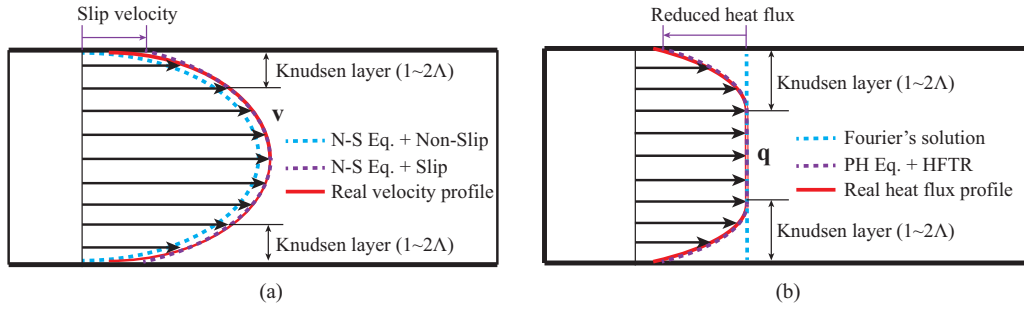


FIG. 5. Schematic of nonequilibrium effects and hydrodynamic modeling in the micro/nanoscale gas flow and phonon flow in the slip regime. (a) The gas flow. The light blue dashed line and purple dashed line represent the solutions of the Navier-Stokes equation (N-S Eq.) with the nonslip velocity boundary condition and velocity slip boundary condition, respectively. The red solid line denotes the real velocity profile. (b) The phonon flow. The light blue dashed line and purple dashed line represent the solutions of Fourier's law and the present phonon hydrodynamic equation (PH Eq.) with the heat flux tangential retardant (HFTR) boundary condition, respectively. The red solid line denotes the real heat flux profile. The Knudsen layer near the lateral boundary has a thickness of $1 \sim 2$ mean-free paths (Λ).

to introduce uniform resistance throughout the medium so that the heat flux profile becomes a flat one in the diffusive regime, as predicted by Fourier's law. When coming to the micro/nanoscale transport, the physical picture thus becomes diverse. The rarefied interaction between gas molecules and the wall at the micro/nanoscale makes the destruction of molecule momentum insufficient at the wall, which induces a macroscopic gas velocity slip at the wall. However, the boundary shortens the free path of nearby phonons within the Knudsen layer, which induces a further resistance to phonon transport besides the intrinsic resistance by umklapp scattering and thereafter a reduced heat flux at the boundary. The present analysis also corroborates why the "heat flux tangential retardant" (HFTR) boundary condition is introduced in place of the "slip" boundary condition in Sec. III A for nanoscale phonon heat transport.

2. Cross-plane phonon transport through a thin film

For the 1D steady-state cross-plane phonon transport shown in Fig. 2(b), the phonon Boltzmann equation Eq. (2) is rewritten into the equation of phonon radiative transfer (EPRT) [50]:

$$\mu \frac{\partial I(y, \mu)}{\partial y} = \frac{I^{\text{eq}}(y) - I(y, \mu)}{\Lambda}, \quad (66)$$

$$\begin{aligned} I^+(\eta, \mu) &= I^+(0, \mu) \exp\left(-\frac{\eta}{\mu}\right) + \int_0^\eta \frac{I^{\text{eq}}(\eta')}{\mu} \exp\left(\frac{\eta' - \eta}{\mu}\right) d\eta', \quad 0 \leq \mu \leq 1, \\ I^-(\eta, \mu) &= I^-(\xi, \mu) \exp\left(\frac{\xi - \eta}{\mu}\right) - \int_\eta^\xi \frac{I^{\text{eq}}(\eta')}{\mu} \exp\left(\frac{\eta' - \eta}{\mu}\right) d\eta', \quad -1 \leq \mu \leq 0, \end{aligned} \quad (68)$$

where the dimensionless coordinate is defined as $\eta = y/\Lambda$, and the inverse of the spatial Knudsen number is $\xi = 1/\text{Kn}_l = d/\Lambda$. For the fully diffuse isothermal boundaries ($s = 0$), $I^+(0, \mu)$ and $I^-(\xi, \mu)$ are known from the equilibrium distributions at the temperature of hot and cold sources as $I^+(0, \mu) = I^{\text{eq}}(T_h)$ and $I^-(\xi, \mu) = I^{\text{eq}}(T_c)$. For the partially diffuse and partially specular isothermal boundaries ($s \neq 0$), they are determined from Eq. (67) and Eq. (68) (details are shown in the Appendix A):

$$\begin{aligned} I^+(0, \mu) &= \frac{1-s}{1-s^2 \exp(-2\xi/\mu)} I^{\text{eq}}(T_h) + \frac{s(1-s) \exp(-\xi/\mu)}{1-s^2 \exp(-2\xi/\mu)} I^{\text{eq}}(T_c) + \frac{s^2 \exp(-2\xi/\mu)}{1-s^2 \exp(-2\xi/\mu)} \int_0^\xi \frac{I^{\text{eq}}(\eta')}{\mu} \exp\left(\frac{\eta'}{\mu}\right) d\eta' \\ &+ \frac{s}{1-s^2 \exp(-2\xi/\mu)} \int_0^\xi \frac{I^{\text{eq}}(\eta')}{\mu} \exp\left(-\frac{\eta'}{\mu}\right) d\eta', \end{aligned} \quad (69)$$

where the phonon intensity is defined as: $I = \int v_g \hbar \omega f \frac{D(\omega)}{4\pi} d\omega$, with the equilibrium phonon intensity $I^{\text{eq}} = \int v_g \hbar \omega f_R^{\text{eq}} \frac{D(\omega)}{4\pi} d\omega$. $D(\omega)$ is the density of phonon states per unit volume around per unit frequency interval. We consider two isothermal heat sources with partially diffuse and partially specular surfaces. The boundary conditions Eq. (35) for Eq. (66) become

$$\begin{aligned} y = 0, \quad I^+(0, \mu) &= (1-s)I^{\text{eq}}(T_h) + sI^-(0, -\mu), \\ y = d, \quad I^-(d, \mu) &= (1-s)I^{\text{eq}}(T_c) + sI^+(d, -\mu). \end{aligned} \quad (67)$$

The numerical solution of Eq. (66) with the fully diffuse isothermal boundaries [$s = 0$ in Eq. (67)] has been given in the classical monograph [1]. A semianalytical series expansion method was recently developed to solve the frequency-dependent phonon Boltzmann equation for cross-plane heat transport with a variety of isothermal boundary conditions [78]. As the gray phonon transport is considered in the present work, we follow the general idea for the fully diffuse case in Ref. [1] and provide the numerical solution of Eq. (66) with an arbitrary value of specular parameter s in Eq. (67).

The general solution of Eq. (66) is obtained through the integration along its characteristics [1]:

$$\begin{aligned}
 I^-(\xi, \mu) = & \frac{1-s}{1-s^2 \exp(2\xi/\mu)} I^{\text{eq}}(T_c) + \frac{s(1-s) \exp(\xi/\mu)}{1-s^2 \exp(2\xi/\mu)} I^{\text{eq}}(T_h) - \frac{s^2 \exp(2\xi/\mu)}{1-s^2 \exp(2\xi/\mu)} \int_0^\xi \frac{I^{\text{eq}}(\eta')}{\mu} \exp\left(\frac{\eta' - \xi}{\mu}\right) d\eta' \\
 & - \frac{s}{1-s^2 \exp(2\xi/\mu)} \int_0^\xi \frac{I^{\text{eq}}(\eta')}{\mu} \exp\left(\frac{\xi - \eta'}{\mu}\right) d\eta'. \quad (70)
 \end{aligned}$$

Substitution of Eq. (69) and Eq. (70) into Eq. (68) results in the expression of phonon intensity as a function of the integration of equilibrium phonon intensity. With the aid of the relations between phonon intensity and energy density, $I^{\text{eq}} = \frac{v_g}{4\pi} e^{\text{eq}} = \frac{v_g}{4\pi} e$ and $e = \frac{1}{v_g} \int_{4\pi} I(\eta, \mu) d\Omega$, we derive an integral equation for energy density distribution:

$$2e^*(\eta) = G(\eta) + \int_0^\xi e^*(\eta') \int_0^1 F(\eta', \eta, \mu) d\mu d\eta', \quad (71)$$

where the dimensionless energy density has been defined as $e^*(\eta) \equiv \frac{e(\eta) - e(T_c)}{e(T_h) - e(T_c)}$. The function $G(\eta)$ and integral kernel $F(\eta', \eta, \mu)$ are denoted fully as

$$\begin{aligned}
 G(\eta) = & \int_0^1 \left[\frac{1-s}{1-s^2 \exp(-2\xi/\mu)} \exp\left(-\frac{\eta}{\mu}\right) + \frac{s(1-s)}{1-s^2 \exp(-2\xi/\mu)} \exp\left(\frac{\eta - 2\xi}{\mu}\right) \right] d\mu, \quad (72) \\
 F(\eta', \eta, \mu) = & \frac{1}{\mu} \left\{ \exp\left(-\frac{|\eta' - \eta|}{\mu}\right) + \frac{s}{1-s^2 \exp(-2\xi/\mu)} \left[\exp\left(\frac{\eta' + \eta - 2\xi}{\mu}\right) + \exp\left(-\frac{\eta' + \eta}{\mu}\right) \right] \right. \\
 & \left. + \frac{s^2}{1-s^2 \exp(-2\xi/\mu)} \left[\exp\left(\frac{\eta - \eta' - 2\xi}{\mu}\right) + \exp\left(\frac{\eta' - \eta - 2\xi}{\mu}\right) \right] \right\}. \quad (73)
 \end{aligned}$$

The temperature distribution across the thin film is related to the energy density distribution as $\Theta(Y) = e^*(\eta)$, with $\Theta \equiv \frac{T - T_c}{T_h - T_c}$ and $Y \equiv \eta/\xi = y/d$. The numerical method developed for the case of diffuse isothermal boundaries [1] is applied to solve Eq. (71), with the trapezoidal scheme to compute the integration over the spatial coordinate η' (the details of the numerical solution are shown in Appendix B). A grid of $N_\eta = 1001$ is used after a verification of grid independence. Based on the kinetic definition, $q_y = \int_{4\pi} \mu I(\eta, \mu) d\Omega$, we obtain the expression of heat flux across the thin film:

$$\begin{aligned}
 q^* = & 2 \int_0^1 \left[\frac{1-s}{1-s^2 \exp(-2\xi/\mu)} \mu - \frac{s(1-s)}{1-s^2 \exp(-2\xi/\mu)} \mu \exp(-2\xi/\mu) + \frac{s-1}{1-s^2 \exp(-2\xi/\mu)} \int_0^\xi e^*(\eta') \exp\left(-\frac{\eta'}{\mu}\right) d\eta' \right. \\
 & \left. + \frac{s(s-1)}{1-s^2 \exp(-2\xi/\mu)} \int_0^\xi e^*(\eta') \exp\left(\frac{\eta' - 2\xi}{\mu}\right) d\eta' \right] d\mu, \quad (74)
 \end{aligned}$$

where the dimensionless heat flux is defined as $q^* \equiv \frac{4q_y}{v_g [e(T_h) - e(T_c)]}$. The effective cross-plane thermal conductivity is defined as $\frac{\lambda_{\text{eff}}}{\lambda_b} = \frac{q_y}{q_b} = \frac{3q_y}{v_g \text{Kn}_l [e(T_h) - e(T_c)]}$, and related to the dimensionless heat flux as

$$\frac{\lambda_{\text{eff}}}{\lambda_b} = \frac{3}{4\text{Kn}_l} q^*. \quad (75)$$

The cross-plane phonon transport through the thin film is also modeled by the phonon hydrodynamic equation Eq. (29), which reduces to the classical Fourier's law since the nonlocal term of heat flux vanishes because of the energy conservation principle: $dq_y/dy = 0$. Thus the temperature differential equation becomes

$$\frac{d^2 T}{dy^2} = 0, \quad (76)$$

with the boundary conditions obtained from Eq. (56):

$$\begin{aligned}
 y = 0, \quad T_h - T = & -\frac{1+s}{1-s} \frac{2}{3} \Lambda \frac{dT}{dy}, \\
 y = d, \quad T - T_c = & -\frac{1+s}{1-s} \frac{2}{3} \Lambda \frac{dT}{dy}. \quad (77)
 \end{aligned}$$

The temperature distribution is then achieved through a solution of Eq. (76) with the boundary conditions Eq. (77):

$$\Theta = \frac{1 + \frac{1+s}{1-s} \frac{2}{3} \text{Kn}_l}{1 + \frac{1+s}{1-s} \frac{4}{3} \text{Kn}_l} - \frac{Y}{1 + \frac{1+s}{1-s} \frac{4}{3} \text{Kn}_l}, \quad (78)$$

where the dimensionless coordinate and temperature have the same definitions as those in phonon Boltzmann equation solutions. The heat flux across the thin film is derived from $q_y = -\lambda dT/dy$ as

$$q_y = \frac{\lambda}{1 + \frac{1+s}{1-s} \frac{4}{3} \text{Kn}_l} \frac{T_h - T_c}{d}. \quad (79)$$

The effective cross-plane thermal conductivity of the thin film is acquired from Eq. (79) as

$$\frac{\lambda_{\text{eff}}}{\lambda_b} = \frac{1}{1 + \frac{1+s}{1-s} \frac{4}{3} \text{Kn}_l}. \quad (80)$$

The comparison of temperature distributions in cross-plane phonon transport is shown in Fig. 6, where an excellent agreement is achieved between the results by the phonon hydrodynamic model and by Boltzmann equation modeling. The temperature jump near the boundaries increases with

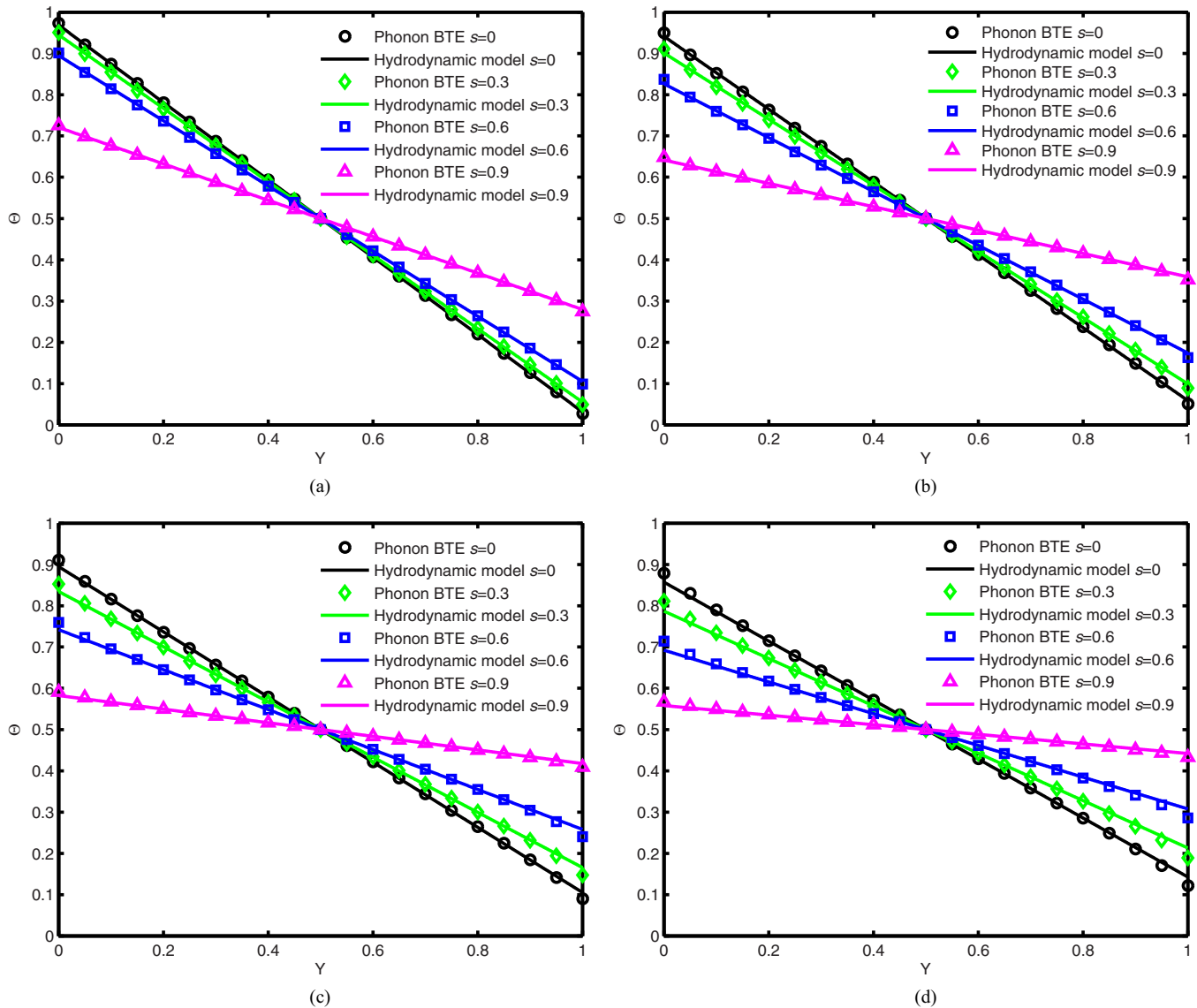


FIG. 6. The dimensionless temperature distributions in the cross-plane phonon transport through the thin film at different spatial Knudsen numbers: (a) $Kn_l = 0.05$, (b) $Kn_l = 0.1$, (c) $Kn_l = 0.2$, (d) $Kn_l = 0.3$. The solid lines represent the analytical solution Eq. (78) based on the present phonon hydrodynamic model, whereas the symbols represent the numerical solution of Eq. (71) based on the phonon Boltzmann transport equation (BTE). Different specularity parameters are considered for the surface of the isothermal heat sources: $s = 0$ (circle), $s = 0.3$ (diamond), $s = 0.6$ (square), $s = 0.9$ (triangle). The spatial Knudsen number is defined as the ratio of phonon mean-free path to the thin-film thickness: $Kn_l \equiv \Lambda/d$.

increasing Kn_l due to the thermodynamic nonequilibrium effect. In addition, a larger temperature jump is obtained at an elevated surface specularity parameter of the heat sources, as induced by less sufficient phonon-boundary thermalization and larger thermal resistance. Therefore, in contrast to the in-plane transport, the effective cross-plane thermal conductivity decreases as the specularity parameter increases, as shown in Fig. 7. In all, the phonon hydrodynamic model produces very accurate temperature distributions at a spatial Knudsen number smaller than about 0.3. On the other hand, the heat flux is predicted still very well when Kn_l reaches as high as 5 or even larger, which has also been obtained in lattice Boltzmann modeling of the same case [79]. Furthermore,

the present model provides a much more efficient approach to the cross-plane heat transport which requires otherwise a very complicated numerical solution of the phonon Boltzmann equation. The phonon hydrodynamic model gives a simple analytical solution as well as a clarified interpretation of the boundary nonequilibrium effects.

3. Phonon transport through a nanowire

For phonon transport through a nanowire as shown in Fig. 8, a uniform temperature gradient $-dT/dx$ is exerted along the nanowire with a lateral surface specularity parameter s . The Boltzmann equation solutions have been already obtained for the same electron transport problem [80], where the radial heat

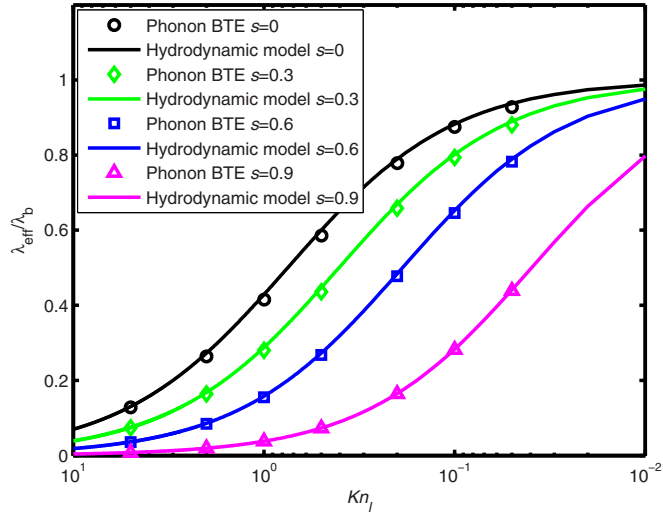


FIG. 7. The dimensionless effective cross-plane thermal conductivity of the thin film. The solid lines represent the analytical solution Eq. (80) based on the present phonon hydrodynamic model, whereas the symbols represent the numerical solution Eq. (75) based on the phonon Boltzmann transport equation (BTE). Different specular parameters are considered for the surface of isothermal heat sources: $s = 0$ (circle), $s = 0.3$ (diamond), $s = 0.6$ (square), $s = 0.9$ (triangle). The spatial Knudsen number is defined as the ratio of the phonon mean-free path to the thin-film thickness: $\text{Kn}_l \equiv \Lambda/d$.

flux distribution is

$$q^*(r^*) = 1 - \frac{3}{4\pi}(1-s) \sum_{n=0}^{\infty} s^n \int_0^{\pi} d\theta \cos^2\theta \sin\theta \int_0^{2\pi} d\varphi \times \exp\left[-\frac{r^* \sin\varphi + (2n+1)\sqrt{1-r^{*2}\cos^2\varphi}}{\text{Kn}_l \sin\theta}\right], \quad (81)$$

where the dimensionless radial coordinate and heat flux are defined respectively as $r^* \equiv r/R$ and $q^*(r^*) \equiv \frac{q_x(r)}{-\lambda \frac{dT}{dx}}$, with the spatial Knudsen number $\text{Kn}_l = \Lambda/R$. The effective thermal conductivity of the nanowire is therefore obtained as [80]

$$\frac{\lambda_{\text{eff}}}{\lambda_b} = 1 - \frac{12}{\pi}(1-s)^2 \sum_{n=1}^{\infty} n s^{n-1} \int_0^1 \sqrt{1-t^2} \times \int_0^1 \exp\left(-\frac{n\kappa t}{u}\right) \sqrt{1-u^2} u du dt, \quad (82)$$

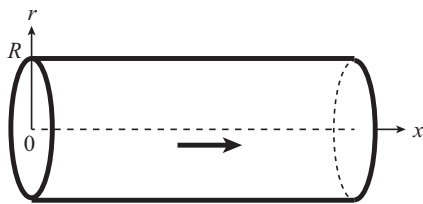


FIG. 8. Schematic of phonon transport through a nanowire with radius R .

where κ is related to the inverse of the spatial Knudsen number as $\kappa = 2/\text{Kn}_l$.

This phonon heat transport is also modeled by the phonon hydrodynamic model Eq. (29), which reduces to

$$\frac{1}{5}\Lambda^2 \frac{d^2 q_x(r)}{dr^2} + \frac{1}{5}\Lambda^2 \frac{1}{r} \frac{dq_x(r)}{dr} - q_x(r) = \lambda \frac{dT}{dx}. \quad (83)$$

Equation (83) is a second-order ordinary differential equation of heat flux, which needs two boundary conditions:

$$\begin{aligned} r = 0, \quad \frac{dq_x(r)}{dr} &= 0, \\ r = R, \quad q_x(r) &= -\frac{1+s}{1-s} \frac{8}{15} \Lambda \frac{dq_x(r)}{dr}. \end{aligned} \quad (84)$$

The general solution of the Bessel equation (83) is $q_x(r) = C_1 J_0(i\sqrt{5}r/\Lambda) - \lambda \frac{dT}{dx}$, where the zeroth-order Bessel function is defined as $J_0(ix) = \sum_{k=0}^{\infty} (x/2)^{2k}/(k!k!)$. The first boundary condition in Eq. (84) has been naturally satisfied. The coefficient C_1 is determined from the second boundary condition in Eq. (84), and the radial heat flux distribution solution is acquired as

$$q^*(r^*) = 1 - \frac{J_0(i\frac{\sqrt{5}}{\text{Kn}_l} r^*)}{J_0(i\frac{\sqrt{5}}{\text{Kn}_l}) - \frac{1+s}{1-s} \frac{8}{3\sqrt{5}} i J_1(i\frac{\sqrt{5}}{\text{Kn}_l})}, \quad (85)$$

where the first-order Bessel function is defined as $J_1(ix) = i \sum_{k=0}^{\infty} (x/2)^{2k+1}/[k!(k+1)!]$. The effective thermal conductivity of the nanowire is obtained through integrating the heat flux over the whole cross section: $\lambda_{\text{eff}}/\lambda_b = (\int_0^R q_x(r) 2\pi r dr)/(-\lambda \frac{dT}{dx} \pi R^2) = 2 \int_0^1 q^*(r^*) r^* dr^*$, which gives rise to the following result when putting Eq. (85) inside:

$$\frac{\lambda_{\text{eff}}}{\lambda_b} = 1 + \frac{\frac{2\text{Kn}_l}{\sqrt{5}} i J_1(i\frac{\sqrt{5}}{\text{Kn}_l})}{J_0(i\frac{\sqrt{5}}{\text{Kn}_l}) - \frac{1+s}{1-s} \frac{8}{3\sqrt{5}} i J_1(i\frac{\sqrt{5}}{\text{Kn}_l})}. \quad (86)$$

The radial heat flux distributions and effective thermal conductivity of phonon transport through the nanowire are shown in Fig. 9 and Fig. 10, respectively, where comparisons are made between the present hydrodynamic modeling results and Boltzmann equation solutions. An appreciably good agreement between them is achieved at a spatial Knudsen number smaller than about 0.3. Similarly to in-plane phonon transport through a thin film, there is a heat flux reduction near the lateral surface at increasing Kn_l due to the thermodynamic nonequilibrium effect. The amount of reduction is larger at a smaller surface specular parameter, resulting in a smaller effective thermal conductivity as seen in Fig. 10.

B. Transient nanoscale heat transport

1. 1D transient phonon transport across a thin film

For the 1D transient phonon transport across a thin film shown in Fig. 11(a), the thin film is initially at a uniform temperature T_c . Suddenly the left-hand side of thin film comes in contact with a hot source at a constant temperature $T_h > T_c$, while the right-hand side comes in contact with a cold source at a constant temperature T_c . Fully diffuse surfaces are considered for both the hot and cold sources. The solution of the phonon

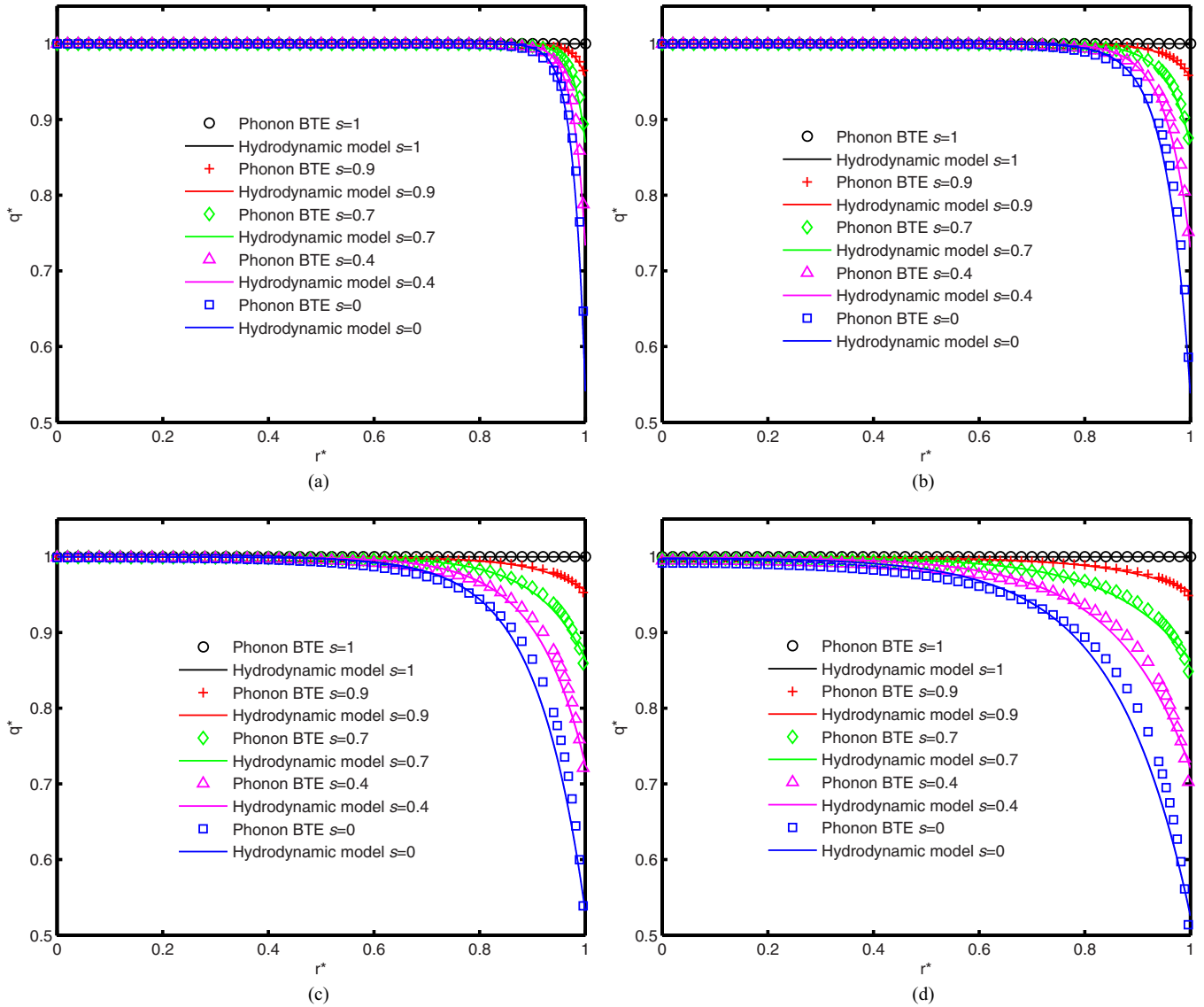


FIG. 9. The dimensionless cross-sectional heat flux distributions for phonon transport through a nanowire at different spatial Knudsen numbers: (a) $Kn_l = 0.05$, (b) $Kn_l = 0.1$, (c) $Kn_l = 0.2$, (d) $Kn_l = 0.3$. The solid lines represent the analytical solution Eq. (85) based on the present phonon hydrodynamic model, whereas the symbols represent the analytical solution Eq. (81) based on the phonon Boltzmann transport equation (BTE). Different specularities parameters are considered for the lateral surface of the nanowire: $s = 1$ (circle), $s = 0.9$ (plus), $s = 0.7$ (diamond), $s = 0.4$ (triangle), $s = 0$ (square). The spatial Knudsen number is defined as the ratio of the phonon mean-free path to the nanowire radius: $Kn_l \equiv \Lambda/R$.

Boltzmann equation for this problem has been obtained by the discrete ordinate method (DOM) in previous work [36,81]. For a convenient comparison, we use an efficient energy-based deviational Monte Carlo method [51,82] to solve the phonon Boltzmann equation.

This transient phonon transport problem is also modeled by the present phonon hydrodynamic model, with the heat transport equation (29) and energy balance Eq. (5) reducing to respectively

$$\frac{\partial q^*}{\partial \tau} + q^* = -\frac{1}{3}Kn_l \frac{\partial \Theta}{\partial X} + \frac{4}{15}Kn_l^2 \frac{\partial^2 q^*}{\partial X^2}, \quad (87)$$

$$\frac{\partial \Theta}{\partial \tau} = -Kn_l \frac{\partial q^*}{\partial X}, \quad (88)$$

where the dimensionless time, spatial coordinate, temperature, and heat flux have been introduced separately as $\tau \equiv t/\tau_R$, $X \equiv x/d$, $\Theta \equiv (T - T_c)/(T_h - T_c)$, $q^* \equiv q_x/[v_g C_V(T_h - T_c)]$, and the spatial Knudsen number is defined as $Kn_l = \Lambda/d$. A temporal Knudsen number is introduced as the ratio of phonon relaxation time to characteristic time: $Kn_t = \tau_R/t$ (the inverse of dimensionless time). The dimensionless temperature differential equation is obtained by combining Eq. (87) and Eq. (88):

$$\frac{\partial^2 \Theta}{\partial \tau^2} + \frac{\partial \Theta}{\partial \tau} = \frac{1}{3}Kn_l^2 \frac{\partial^2 \Theta}{\partial X^2} + \frac{4}{15}Kn_l^2 \frac{\partial^3 \Theta}{\partial X^2 \partial \tau}. \quad (89)$$

The dimensionless initial conditions for Eq. (89) are $\tau = 0$, $\Theta = 0$, $\partial \Theta / \partial \tau = 0$. The temperature jump boundary conditions Eq. (57) are adopted, with their dimensionless forms

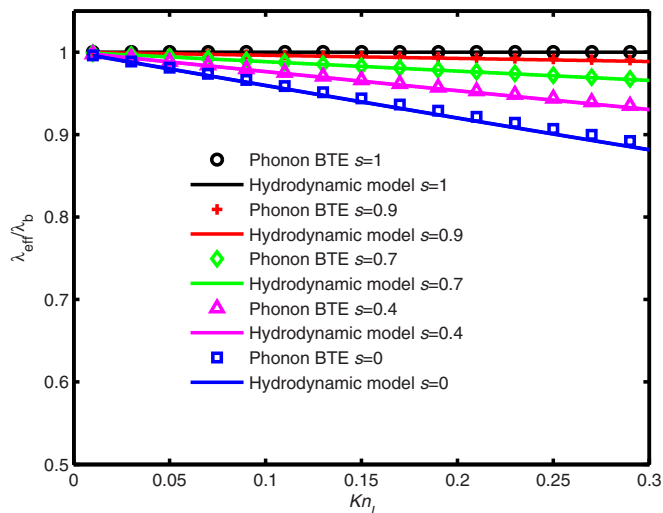


FIG. 10. The dimensionless effective thermal conductivity of the nanowire. The solid lines represent the analytical solution Eq. (86) based on the present phonon hydrodynamic model, whereas the symbols represent the analytical solution Eq. (82) based on the phonon Boltzmann transport equation (BTE). Different specularly parameters are considered for the lateral surface of the nanowire: $s = 1$ (circle), $s = 0.9$ (plus), $s = 0.7$ (diamond), $s = 0.4$ (triangle), $s = 0$ (square). The spatial Knudsen number is defined as the ratio of the phonon mean-free path to the nanowire radius: $\text{Kn}_l \equiv \Lambda/R$.

given as

$$\begin{aligned} X = 0, \quad \Theta - 1 &= \frac{2}{3} \text{Kn}_l \frac{\partial \Theta}{\partial X}, \\ X = 1, \quad \Theta &= -\frac{2}{3} \text{Kn}_l \frac{\partial \Theta}{\partial X}. \end{aligned} \quad (90)$$

A Laplace transform method is applied to solve Eq. (89), where the Laplace transform of temperature distribution is $\tilde{\Theta}(X; p) = \int_0^\infty \Theta(X, \tau) \exp(-p\tau) d\tau$, with p being a complex parameter. In this way, the partial differential equation (PDE) Eq. (89) of $\Theta(X, \tau)$ reduces to an ordinary differential equation (ODE) of $\tilde{\Theta}(X; p)$ in terms of the spatial coordinate X . The analytical solution of dimensionless temperature distribution in the frequency domain is obtained when supplemented with the Laplace transform of boundary conditions Eq. (90). The dimensionless temperature distribution in the real domain is then computed through an inverse Laplace transform via a Riemann-sum approximation [83]. After obtaining the solution of temperature distribution evolution, the heat flux distribution evolution is related to the former based on the Laplace transforms of Eq. (87) and Eq. (88). The mathematical details of the solution of the phonon hydrodynamic model for 1D transient phonon transport across a thin film are provided in Appendix C. To demonstrate the advantage of the present hydrodynamic model, we also include the analytical solutions of the classical Fourier's law and C-V type heat transport law for comparison. The analytical solution of Fourier's law can be found in Ref. [79] whereas the analytical solution of the C-V law is obtained also by the Laplace transform method. Another well-known non-Fourier model for ultrafast heat conduction, the dual-phase-lag (DPL) model [18,83], is not included here for comparison because it involves two

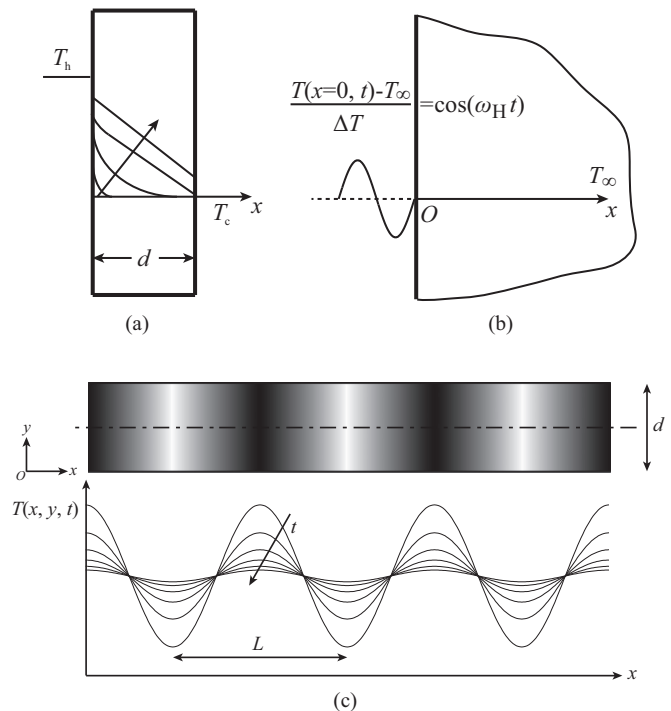


FIG. 11. Schematic of transient nanoscale heat transport: (a) 1D transient phonon transport across the thin film; (b) high-frequency periodic heating of a semi-infinite surface; (c) heat conduction in the transient thermal grating (TTG) experiment.

empirical phase lags which have usually to be determined by adjusting to experimental data of the thermal response [3].

The temporal evolutions of temperature distribution and heat flux distribution across the thin film are shown in Fig. 12 and Fig. 13, respectively. When the thin-film thickness is large such that the spatial Knudsen number is vanishingly small, both the phonon hydrodynamic model and the C-V law recover the Fourier's solutions, as seen in Fig. 12(a) and Fig. 13(a). With decreasing film thickness and increasing spatial Knudsen number, the Fourier's law becomes no longer available due to the thermodynamic nonequilibrium effects from both spatial and temporal aspects. At the early heating stage (a finite temporal Knudsen number), there is a large temperature jump at $X = 0$ caused by the insufficient interaction between the hot source and thin film due to both short time duration and small space dimension, as shown in Figs. 12(b)–12(d). The temperature jump at $X = 0$ gradually decreases with time because of the temporal accumulation of the thermalization between the hot source and thin film. The temporal nonequilibrium effect vanishes when the process reaches the final steady state, with merely the spatial nonequilibrium effect left. Therefore, the temperature jump on both sides of the thin film reduces to the value in steady-state cross-plane phonon transport through the thin film in Sec. IV A 2. The C-V type law shows an improvement over the Fourier's law in capturing the front of the heat propagation attributed to the relaxation term of the heat flux, yet it reduces to the Fourier's law in the steady state. In contrast, the present phonon hydrodynamic model describes well these non-Fourier features and provides good predictions consistent with the Monte Carlo solutions of the phonon Boltzmann equation, as

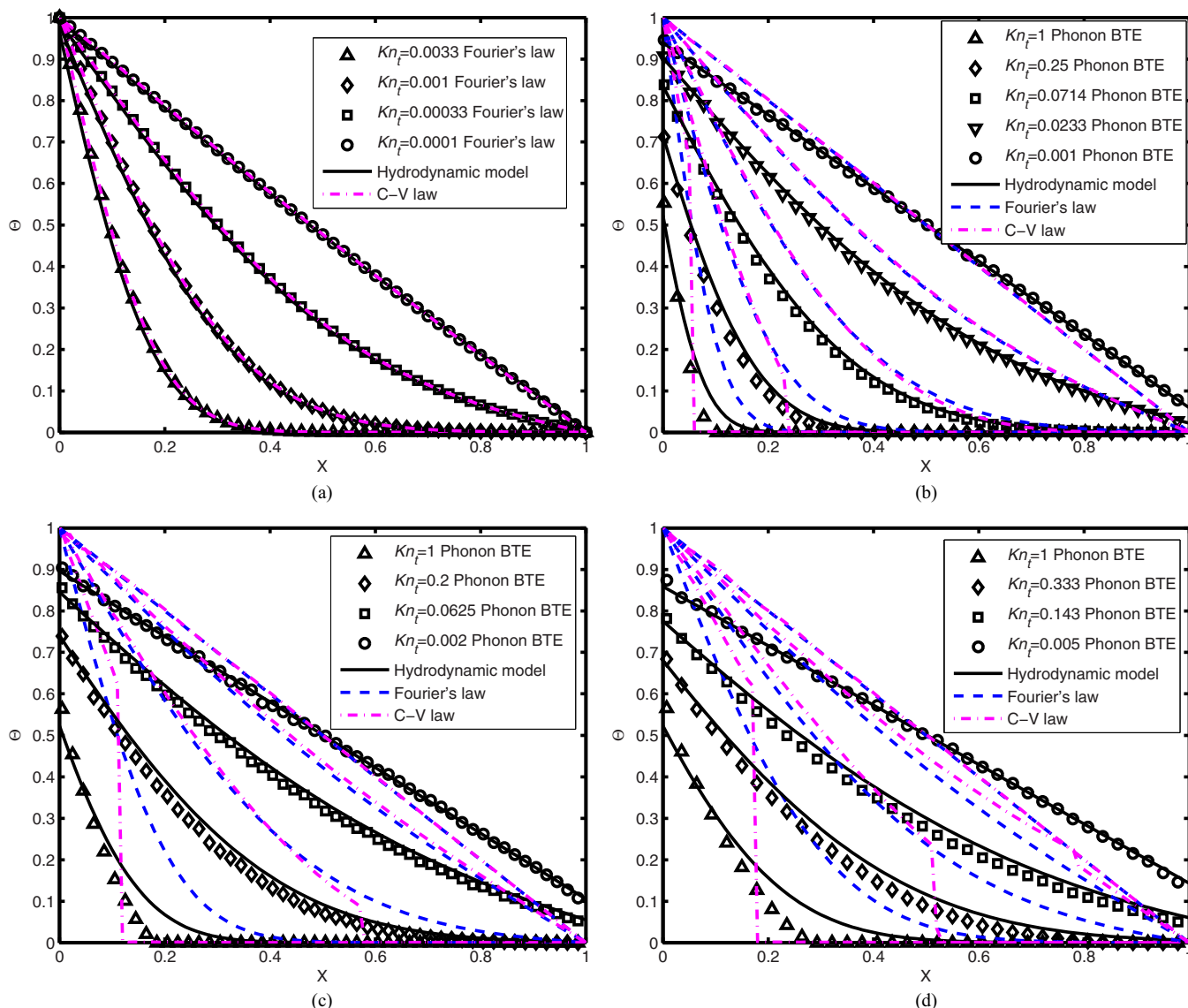


FIG. 12. The temporal evolutions of the dimensionless temperature distribution for the 1D transient phonon transport across the thin film at different spatial Knudsen numbers: (a) $Kn_t = 0.01$, (b) $Kn_t = 0.1$, (c) $Kn_t = 0.2$, (d) $Kn_t = 0.3$. The solid lines and dashed-dotted lines represent the analytical solutions based on the present phonon hydrodynamic model and C-V law, respectively, whereas the symbols represent the analytical solution based on Fourier's law [79] in (a) or the energy-based deviational Monte Carlo solution of the phonon Boltzmann transport equation (BTE) in (b)–(d). The dashed lines represent the analytical solution based on Fourier's law [79] in (b)–(d). The temporal Knudsen number is defined as the ratio of phonon relaxation time to the characteristic time (inverse of the dimensionless time), $Kn_t = \tau_R/t$, whereas the spatial Knudsen number is defined as the ratio of the phonon mean-free path to the thin-film thickness, $Kn_l = \Lambda/d$.

shown in Figs. 12(b)–12(d) and Figs. 13(b)–13(d). The phonon hydrodynamic model works well when both the spatial and temporal Knudsen numbers are smaller than about 0.3, i.e., up to the early transition regime, and can still capture the transient phonon behavior up to $Kn_t = 1$.

2. High-frequency periodic heating of a semi-infinite surface

For the phonon transport in high-frequency periodic heating of a semi-infinite surface shown in Fig. 11(b), the medium is initially at a uniform temperature T_∞ . Suddenly, the left-hand side surface comes in contact with a heat source with a cosine temperature variation versus time. After a sufficiently long

time, the system reaches a quasisteady state independent of the initial condition. A fully diffuse surface is considered for the heat source. The solution of the phonon Boltzmann equation for this problem has been recently obtained by a two-flux method, which gives the temporal evolution of the temperature distribution at the quasisteady state as [71]

$$\Theta(X, \tau) = \frac{1}{2} \sqrt{1 + 2c \cos \psi + c^2} \exp(-\sqrt{3}bX) \times \cos(Kn_t \tau - \sqrt{3}aX + \phi_1), \tag{91}$$

where the dimensionless time and spatial coordinate is defined as $\tau = t/\tau_R$ and $X = x/\Lambda$, with the dimension-

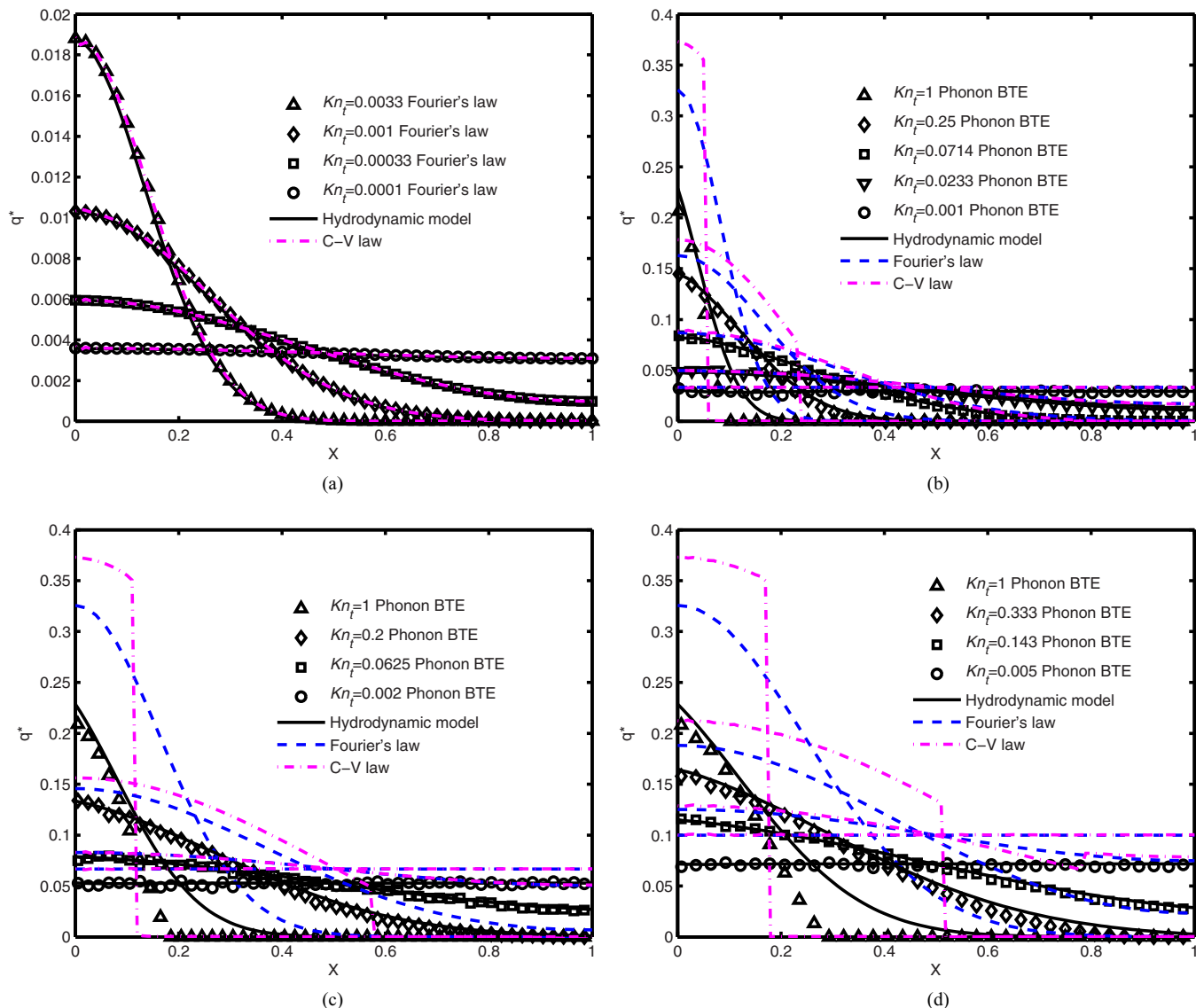


FIG. 13. Temporal evolutions of dimensionless heat flux distribution for the 1D transient phonon transport across the thin film at different spatial Knudsen numbers: (a) $Kn_t = 0.01$, (b) $Kn_t = 0.1$, (c) $Kn_t = 0.2$, (d) $Kn_t = 0.3$. The solid lines and dashed-dotted lines denote the analytical solution based on the present phonon hydrodynamic model and C-V law, respectively, whereas the symbols represent the analytical solution based on Fourier's law [79] in (a) or the energy-based deviational Monte Carlo solution of the phonon Boltzmann transport equation (BTE) in (b)–(d). The dashed lines represent the analytical solution based on Fourier's law [79] in (b)–(d). The temporal Knudsen number is defined as the ratio of the phonon relaxation time to the characteristic time (inverse of the dimensionless time), $Kn_t = \tau_R/t$, whereas the spatial Knudsen number is defined as the ratio of the phonon mean-free path to the thin-film thickness, $Kn_t = \Lambda/d$.

less temperature being $\Theta(X, \tau) = [T(x, t) - T_\infty]/\Delta T$. The parameters in Eq. (91) separately are represented fully as $\cos \psi = b/a$, $\sin \psi = -2b$, $c = b/(a + Kn_t)$, $\tan \phi_1 = c \sin \psi / (1 + c \cos \psi)$, with $a = \sqrt{\frac{Kn_t}{2}} \sqrt{Kn_t + \sqrt{(Kn_t)^2 + 1}}$, $b = \sqrt{\frac{Kn_t}{2}} \sqrt{-Kn_t + \sqrt{(Kn_t)^2 + 1}}$. The temporal Knudsen number is defined as the ratio of phonon relaxation time to the period of external cosine temperature oscillation (inverse of its frequency): $Kn_t = \omega_H \tau_R$, which characterizes the temporal thermodynamic nonequilibrium effect in high-frequency transient heat conduction. The temporal evolution of heat flux distribution at the quasisteady state has been obtained

as [71]

$$q^*(X, \tau) = \frac{1}{2\sqrt{3}} \sqrt{1 - 2c \cos \psi + c^2} \exp(-\sqrt{3}bX) \times \cos(Kn_t \tau - \sqrt{3}aX - \phi_2), \quad (92)$$

where the dimensionless heat flux is defined as $q^*(X, \tau) \equiv q_x(x, t)/v_g C_V \Delta T$, and the parameter $\tan \phi_2 = c \sin \psi / (1 - c \cos \psi)$. In the low-frequency limit with negligible temporal nonequilibrium effect, the Boltzmann equation solutions Eqs. (91) and (92) reduce to the Fourier's solution: $\Theta(X, \tau) = \exp(-\sqrt{3}Kn_t/2X) \cos(Kn_t \tau - \sqrt{3}Kn_t/2X)$ and $q^*(X, \tau) = \sqrt{Kn_t/3} \exp(-\sqrt{3}Kn_t/2X) \cos(Kn_t \tau - \sqrt{3}Kn_t/2X + \pi/4)$.

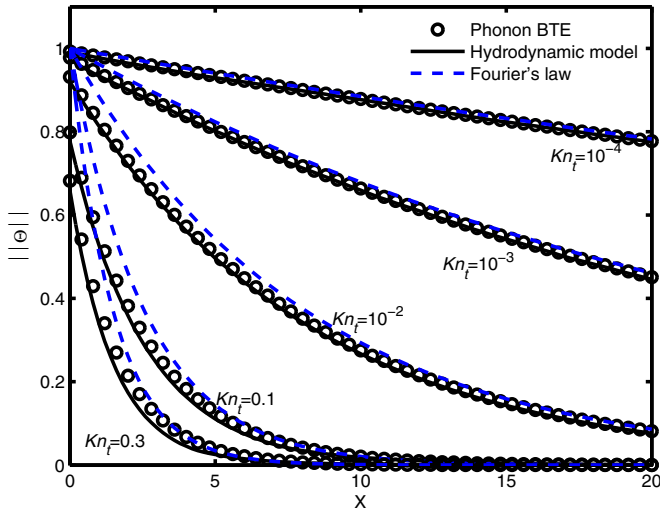


FIG. 14. Spatial distribution of the amplitude of the dimensionless temperature oscillation for the high-frequency periodic heating of the semi-infinite surface at different frequencies. Circles represent the phonon Boltzmann transport equation (BTE) solution from Eq. (91), whereas the solid lines and dashed lines represent the analytical solution of the phonon hydrodynamic model and Fourier's law, respectively. Five different frequencies are considered: $\text{Kn}_t = 10^{-4}$, $\text{Kn}_t = 10^{-3}$, $\text{Kn}_t = 10^{-2}$, $\text{Kn}_t = 0.1$, $\text{Kn}_t = 0.3$. The temporal Knudsen number is defined as the ratio of the phonon relaxation time to the period of external cosine temperature oscillation (inverse of its frequency): $\text{Kn}_t = \omega_H \tau_R$.

This periodic heating problem can be also described by the present phonon hydrodynamic model, with the heat transport equation (29) and energy balance Eq. (5) reducing to respectively

$$\frac{\partial q^*}{\partial \tau} + q^* = -\frac{1}{3} \frac{\partial \Theta}{\partial X} + \frac{4}{15} \frac{\partial^2 q^*}{\partial X^2}, \quad (93)$$

$$\frac{\partial \Theta}{\partial \tau} = -\frac{\partial q^*}{\partial X}, \quad (94)$$

where the definitions of dimensionless variables are the same as those in Eq. (91) and Eq. (92). A combination of Eq. (93) and Eq. (94) results in the temperature differential equation as

$$\frac{\partial^2 \Theta}{\partial \tau^2} + \frac{\partial \Theta}{\partial \tau} = \frac{1}{3} \frac{\partial^2 \Theta}{\partial X^2} + \frac{4}{15} \frac{\partial^3 \Theta}{\partial X^2 \partial \tau}. \quad (95)$$

The dimensionless initial conditions for Eq. (95) are $\tau = 0$, $\Theta = 0$, $\partial \Theta / \partial \tau = 0$. For the boundary conditions, the temperature jump ones are taken into account:

$$\begin{aligned} X = 0, \quad \Theta - \frac{2}{3} \frac{\partial \Theta}{\partial X} &= \cos(\text{Kn}_t \tau), \\ X \rightarrow \infty, \quad \Theta &= 0. \end{aligned} \quad (96)$$

Again a Laplace transform method is applied to solve Eq. (95), with the mathematical details given in Appendix D.

We compare the results of phonon hydrodynamic model to both the phonon Boltzmann equation solution and the Fourier's solution. The amplitude of periodic oscillation of dimensionless temperature distribution throughout the semi-infinite medium is shown in Fig. 14. With increasing heating frequency of the external heat source and temporal Knudsen number, the

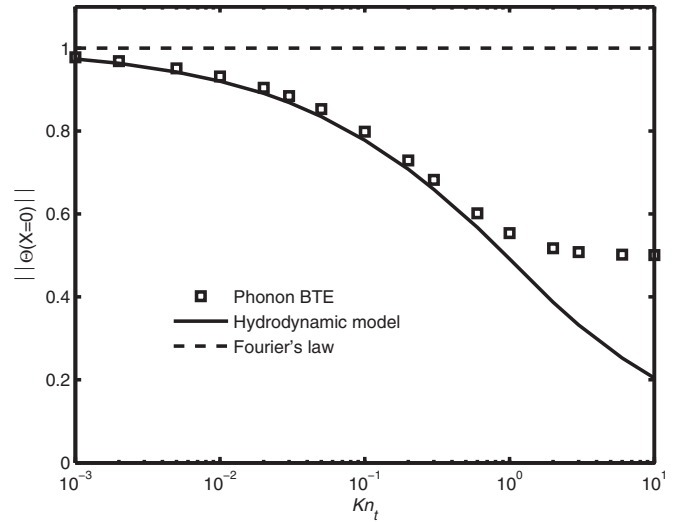


FIG. 15. Heating-frequency dependence of the amplitude of the dimensionless surface temperature oscillation for the high-frequency periodic heating of the semi-infinite surface. The squares represent the phonon Boltzmann transport equation (BTE) solution from Eq. (91), whereas the solid line and dashed line represent the analytical solution of the phonon hydrodynamic model and Fourier's law, respectively. The temporal Knudsen number is defined as the ratio of the phonon relaxation time to the period of external cosine temperature oscillation (inverse of its frequency): $\text{Kn}_t = \omega_H \tau_R$.

heating-influenced region becomes smaller. Furthermore, an appreciable surface temperature jump is obtained at a heating frequency comparable to the inverse of phonon relaxation time, which can no longer be described by the Fourier's law. This nonequilibrium phenomenon comes from the insufficient interaction between the heat source and the medium in such a short period of the temperature oscillation that the surface cannot approach the temperature of the heat source. It has a different origin but the same manifestation compared with the usual temperature jump due to small system size, which indicates the equivalent role of the temporal nonequilibrium effect to the spatial one in non-Fourier heat conduction. The amount of the surface temperature jump increases with the temporal Knudsen number, as further demonstrated in Fig. 15. The phonon hydrodynamic model is capable of describing accurately these transient non-Fourier features at a temporal Knudsen number smaller than about 0.3. A surprising good prediction of the amplitude of the surface heat flux oscillation at the temporal Knudsen number even as large as 10 is obtained in Fig. 16, similar to the result (cf. Fig. 7) in steady-state cross-plane phonon transport through a thin film in Sec. IV A 2.

3. Heat conduction in a transient thermal grating

For phonon heat conduction in transient thermal grating (TTG) along a thin film shown in Fig. 11(c), an initial periodic temperature distribution (thermal grating) is given as $T(x, t = 0) = T_m \cos(qx)$ [84], with T_m the initial amplitude, and wave number q related to the grating period L as $q = 2\pi/L$. The TTG heat conduction is an intricate process as there exist cross-coupling thermodynamic nonequilibrium effects from both phonon-boundary confinement due to finite film

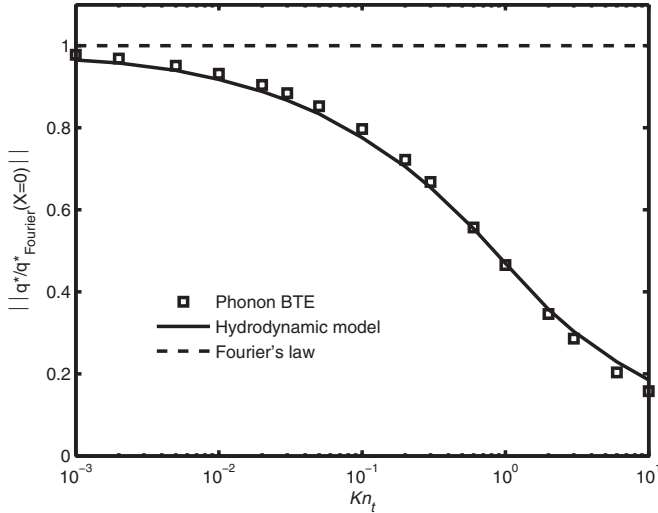


FIG. 16. Heating-frequency dependence of the amplitude of the dimensionless surface heat flux oscillation for the high-frequency periodic heating of the semi-infinite surface. The squares represent the phonon Boltzmann transport equation (BTE) solution from Eq. (92), whereas the solid line and dashed line represent the analytical solution of the phonon hydrodynamic model and Fourier's law, respectively. The temporal Knudsen number is defined as the ratio of the phonon relaxation time to the period of external cosine temperature oscillation (inverse of its frequency): $\text{Kn}_t = \omega_H \tau_R$.

thickness and quasiballistic transport due to finite grating period. They are characterized by the spatial Knudsen number $\text{Kn}_l = \Lambda/d$ and inverse nondimensional grating period $\eta = 2\pi \Lambda/L$, respectively [84]. Thus the theoretical modeling of TTG heat conduction is a challenging task, which involves a complicated numerical solution of the phonon Boltzmann equation in recent work [66,84]. In contrast, the present phonon hydrodynamic model provides a simple and efficient avenue to this problem, through an analytical solution of Eq. (5) and Eq. (29) with the HFTR boundary condition. A fully diffuse surface is assumed for the thin film [84].

It is reasonable to assume the temperature distribution along the thin film remains periodic throughout the decay process as shown in Fig. 11(c). Due to enhanced boundary scattering of phonons near the film surface, the decay rate of temperature amplitude is smaller in the vicinity of lateral boundary. The temperature distribution along the cross-sectional direction will become nonuniform [66]. Thus the TTG heat conduction is a two-dimensional transient process, where the temperature distribution evolves as $T = \langle T(y,t) \rangle \cos(qx)$ with $\langle T(y,t) \rangle$ denoting the amplitude of temperature distribution. The heat flux along the thin film is also periodic, yet with a phase delay behind the temperature distribution: $q_x = -\langle q_x(y,t) \rangle \sin(qx)$ with $-\langle q_x(y,t) \rangle$ denoting the amplitude of heat flux along the thin film. Due to the nonuniform temperature distribution along the cross-sectional direction, a heat flux is induced as $q_y = \langle q_y(y,t) \rangle \cos(qx)$ with $\langle q_y(y,t) \rangle$ the amplitude of heat flux in the cross-sectional direction. Substituting the periodic expressions of temperature and heat flux distributions into the phonon hydrodynamic Eq. (29) and energy balance Eq. (5), we obtain the governing equations for their

amplitudes:

$$\begin{aligned} \frac{\partial q_x^*}{\partial \tau} + \left(1 + \frac{4}{15}\eta^2\right)q_x^* \\ = -\frac{1}{3}\eta^2\theta + \frac{1}{5}\text{Kn}_l^2 \frac{\partial^2 q_x^*}{\partial Y^2} + \frac{1}{15}\eta^2 \frac{\partial q_y^*}{\partial Y}, \end{aligned} \quad (97)$$

$$\begin{aligned} \frac{\partial q_y^*}{\partial \tau} + \left(1 + \frac{1}{5}\eta^2\right)q_y^* \\ = -\frac{1}{3}\text{Kn}_l^2 \frac{\partial \theta}{\partial Y} + \frac{4}{15}\text{Kn}_l^2 \frac{\partial^2 q_y^*}{\partial Y^2} - \frac{1}{15}\text{Kn}_l^2 \frac{\partial q_x^*}{\partial Y}, \end{aligned} \quad (98)$$

$$\frac{\partial \theta}{\partial \tau} = q_x^* - \frac{\partial q_y^*}{\partial Y}, \quad (99)$$

wherein the nondimensional variables are introduced as

$$\begin{aligned} Y = \frac{y}{d}, \quad \tau = \frac{t}{\tau_R}, \quad \theta(Y, \tau) = \frac{\langle T(y,t) \rangle}{T_m}, \\ q_x^*(Y, \tau) = \frac{\langle q_x(y,t) \rangle}{C_V T_m / \tau_R q}, \quad q_y^*(Y, \tau) = \frac{\langle q_y(y,t) \rangle}{C_V T_m d / \tau_R}. \end{aligned} \quad (100)$$

The initial conditions and boundary conditions for Eqs. (97)–(99) are respectively

$$\tau = 0, \quad \theta = 1, \quad \frac{\partial \theta}{\partial \tau} = 0; \quad q_x^* = 0, \quad q_y^* = 0, \quad (101)$$

$$Y = 0, \quad q_x^* = \frac{8}{15}\text{Kn}_l \frac{\partial q_x^*}{\partial Y}, \quad q_y^* = 0,$$

$$Y = \frac{1}{2}, \quad \frac{\partial q_x^*}{\partial Y} = 0, \quad q_y^* = 0. \quad (102)$$

A Laplace transform method is applied to solve Eqs. (97)–(99), which thereafter reduce to a set of ordinary differential equations. Furthermore, we get a fourth-order differential equation of x -direction heat flux amplitude by eliminating the y -direction heat flux amplitude and temperature amplitude:

$$\frac{d^4 \bar{q}_x^*}{dY^4} + F \frac{d^2 \bar{q}_x^*}{dY^2} + G \bar{q}_x^* + H = 0, \quad (103)$$

wherein $\bar{q}_x^*(Y; p) = \int_0^\infty q_x^*(Y, \tau) \exp(-p\tau) d\tau$ and $F = AC - B - D$, $G = BD$, $H = DE$, with the parameters fully denoted as

$$\begin{aligned} A \equiv \frac{\frac{1}{3}\eta^2 + \frac{1}{15}p\eta^2}{\frac{1}{5}p\text{Kn}_l^2}, \quad B \equiv \frac{p^2 + p + \frac{4}{15}p\eta^2 + \frac{1}{3}\eta^2}{\frac{1}{5}p\text{Kn}_l^2}, \\ C \equiv \frac{\frac{1}{3} + \frac{1}{15}p}{\frac{1}{3} + \frac{4}{15}p}, \quad D \equiv \frac{p^2 + p + \frac{1}{5}p\eta^2}{\frac{1}{3}\text{Kn}_l^2 + \frac{4}{15}p\text{Kn}_l^2}, \quad E \equiv \frac{\frac{1}{3}\eta^2}{\frac{1}{5}p\text{Kn}_l^2}. \end{aligned} \quad (104)$$

The boundary conditions for Eq. (103) are determined as

$$\begin{aligned} Y = 0, \quad \bar{q}_x^* = \frac{8}{15}\text{Kn}_l \frac{d\bar{q}_x^*}{dY}, \quad \frac{d^3 \bar{q}_x^*}{dY^3} + (AC - B) \frac{d\bar{q}_x^*}{dY} = 0, \\ Y = \frac{1}{2}, \quad \frac{d\bar{q}_x^*}{dY} = 0, \quad \frac{d^3 \bar{q}_x^*}{dY^3} = 0. \end{aligned} \quad (105)$$

The nondimensional x -direction heat flux amplitude in the frequency domain is obtained by solving Eq. (103) supplemented

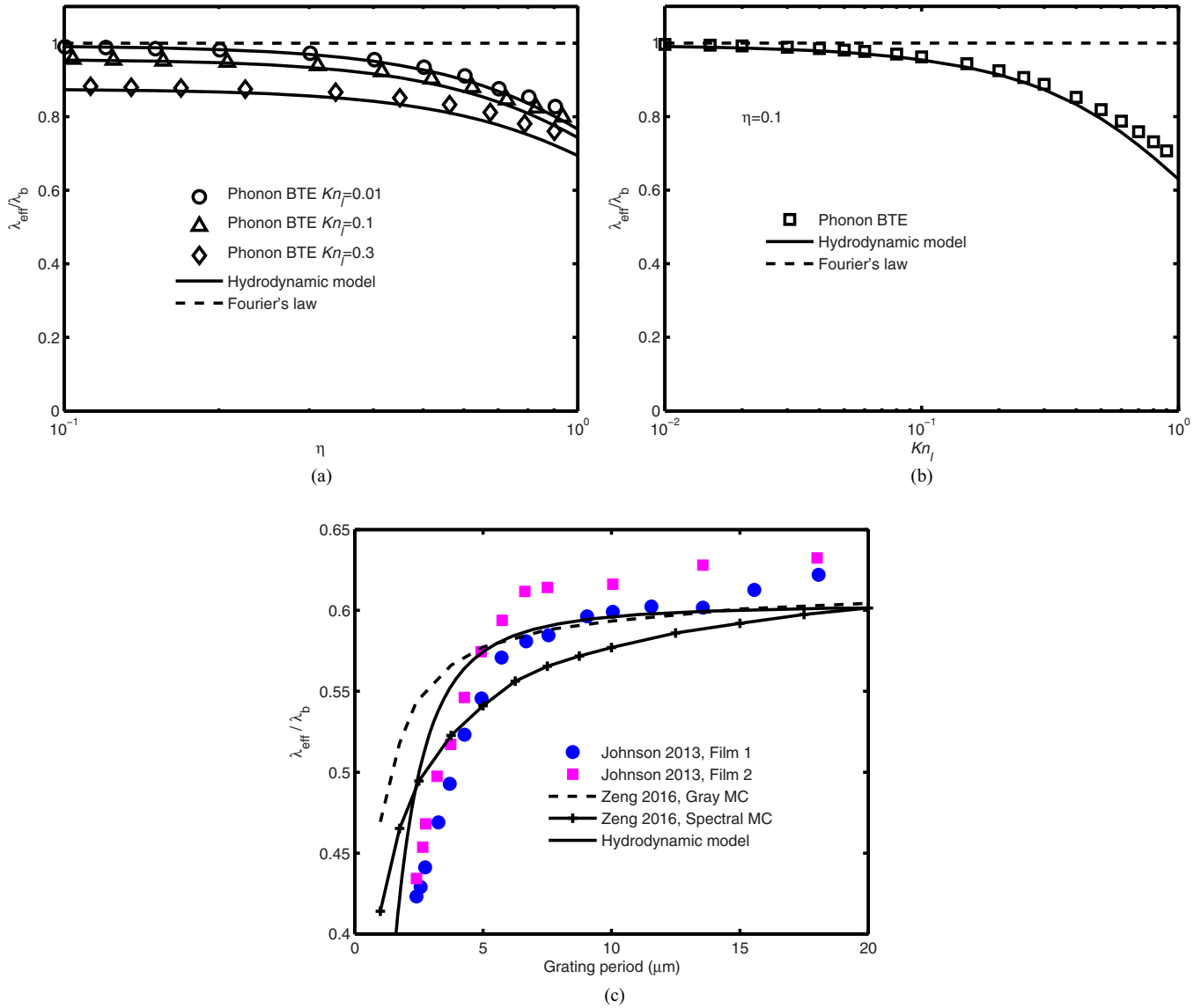


FIG. 17. Nondimensional effective in-plane thermal conductivity of the silicon thin film in the transient thermal grating (TTG) experiment at room temperature ($T = 300$ K). (a) and (b) Comparison to theoretical solutions. The symbols represent the solutions of the phonon Boltzmann transport equation (BTE) [84] whereas the solid line and dashed line denote the analytical solution of the phonon hydrodynamic model and Fourier's law, respectively. The spatial Knudsen number and inverse nondimensional grating period are defined respectively as $Kn_l = \Lambda/d$ and $\eta = 2\pi \Lambda/L$. (c) Comparison to experimental results. The symbols represent the experimental data of two thin films with thickness 400 nm from the literature [72] whereas the solid line represents the results of the present phonon hydrodynamic model with a median-thermal-conductivity phonon MFP $\Lambda_m = 441$ nm [72,77]. The dashed line and solid line with the cross symbol denote the gray and spectral Monte Carlo (MC) solutions of the phonon BTE [84], respectively.

with Eq. (105):

$$\overline{q_x^*} = C_2 \{ \exp(-mY) + \exp[m(Y-1)] \} + C_4 \{ \exp(-nY) + \exp[n(Y-1)] \} - \frac{H}{G}, \quad (106)$$

wherein $m \equiv \{0.5[(F^2 - 4G)^{1/2} - F]\}^{1/2}$, $n \equiv \{-0.5[(F^2 - 4G)^{1/2} + F]\}^{1/2}$, and the two coefficients are specified from the following equations:

$$\begin{aligned} & \left[\frac{[n^3 + (AC - B)n][1 - \exp(-n)]}{[m^3 + (AC - B)m][\exp(-m) - 1]} \left\{ 1 + \exp(-m) + \frac{8}{15} m Kn_l [1 - \exp(-m)] \right\} \right. \\ & \left. + \left(1 - \frac{8}{15} n Kn_l \right) \exp(-n) + \left(1 + \frac{8}{15} n Kn_l \right) \right] C_4 = \frac{H}{G}, \end{aligned} \quad (107)$$

$$C_2 = C_4 \frac{[n^3 + (AC - B)n][1 - \exp(-n)]}{[m^3 + (AC - B)m][\exp(-m) - 1]}. \quad (108)$$

The nondimensional temperature distribution amplitude in the frequency domain is related to the solution of x -direction heat flux amplitude Eq. (106) through

$$\begin{aligned} \bar{\theta}(Y; p) = & \frac{\frac{1}{5}\text{Kn}_l^2}{\frac{1}{3}\eta^2 + \frac{1}{15}p\eta^2} \frac{d^2\bar{q}_x^*}{dY^2} - \frac{p + 1 + \frac{1}{15}\eta^2}{\frac{1}{3}\eta^2 + \frac{1}{15}p\eta^2} \bar{q}_x^* \\ & + \frac{\frac{1}{15}\eta^2}{\frac{1}{3}\eta^2 + \frac{1}{15}p\eta^2}. \end{aligned} \quad (109)$$

An inverse Laplace transform of Eq. (109) based on a Riemannsum approximation [83] produces the temporal evolution of the nondimensional temperature distribution amplitude $\theta(Y, \tau)$. The effective in-plane thermal conductivity of the thin film is then extracted through fitting the decay of the average temperature distribution amplitude along the cross-sectional direction by the diffusion model: $\int_0^1 \theta(Y, \tau) dY = \exp(-\alpha_{\text{eff}} q^2 t)$ [66,84].

The present phonon hydrodynamic model captures well the lateral phonon confinement effect and the in-plane quasiballistic effect simultaneously, as shown in Fig. 17(a). For the case of $\text{Kn}_l = 0.01$, the film thickness is large enough that the phonon-boundary confinement is negligibly small. However, the effective in-plane thermal conductivity of the thin film drops as the grating period decreases or η increases. The recent extended Fourier's continuum model accounting for kinetic effects from boundary inhomogeneity is not available for this heat conduction with internal spatial variation of thermal grating at a characteristic dimension comparable to the phonon MFP [39]. As the correction of the constitutive heat transport equation is considered with additional relaxation and nonlocal terms, the present phonon hydrodynamic model is capable of describing such a quasiballistic effect. The result for the other limit of large grating period is shown in Fig. 17(b), where the present model produces the boundary suppression effect consistent with the Fuchs-Sondheimer model. In all, the rigorous validity of the macroscopic hydrodynamic model is $\text{Kn}_l < 0.3$ and $\eta < 1$. By including the phonon spectral property using the median-thermal-conductivity phonon MFP Λ_m in Sec. IV A 1, the phonon hydrodynamic model provides a prediction of the effective in-plane thermal conductivity of silicon thin film at room temperature in good agreement with recent TTG experimental data [72], as shown in Fig. 17(c). The agreement is encouraging because it not only verifies the idea of employing the median-thermal-conductivity MFP for fast analysis of size effect in Ref. [72], but also demonstrate the power of the macroscopic heat transport model which requires much less computational cost and presents a more clarified physical interpretation.

V. CONCLUSIONS

To conclude, we have developed the phonon hydrodynamics for nanoscale heat transport at ordinary temperatures. The macroscopic model is derived from a perturbation solution to the phonon Boltzmann equation around a nonequilibrium dis-

tribution obtained by entropy maximization. We have demonstrated and validated the phonon hydrodynamic model through modeling extensive extremely small and ultrafast non-Fourier heat conduction. The serious validity of the present model lies in that both the spatial and the temporal Knudsen numbers are smaller than 0.3. The predictions of this model agree well with the experimental results even in a broader range. The macroscopic equations not only provide clear physical interpretation of the thermodynamics nonequilibrium effect at extreme states, but also make feasible the thermal performance optimization of nanosystems pending in future work. Through this work, the phonon hydrodynamic model becomes indispensable for description of heat transport in the sub-continuum and near-transition regimes where Fourier's law fails and a solution of the phonon Boltzmann equation is too expensive. This work represents a crucial step towards macroscopic modeling of nanoscale heat transport, with the phonon spectral properties to be further considered in the future.

ACKNOWLEDGMENTS

This work is financially supported by the NSF of China (Grants No. 91634107 and No. 51621062), and the Key Basic Scientific Research Program (2013CB228301). The authors appreciate very much the helpful discussions with Prof. D. Jou, Prof. S. Y. Chen, and Dr. J.-P. M. Péraud. The deviational Monte Carlo data for transient cross-plane phonon transport and TTG heat conduction through a thin film is provided by X. Ran and Dr. L. P. Zeng, respectively.

APPENDIX A: SOLUTION OF THE BOLTZMANN EQUATION FOR CROSS-PLANE PHONON TRANSPORT THROUGH A THIN FILM

The general solution of Eq. (66) by the method of characteristics is

$$\begin{aligned} I^+(\eta, \mu) = & I^+(0, \mu) \exp\left(-\frac{\eta}{\mu}\right) \\ & + \int_0^\eta \frac{I^{\text{eq}}(\eta')}{\mu} \exp\left(\frac{\eta' - \eta}{\mu}\right) d\eta', \quad 0 \leq \mu \leq 1, \\ I^-(\eta, \mu) = & I^-(\xi, \mu) \exp\left(\frac{\xi - \eta}{\mu}\right) \\ & - \int_\eta^\xi \frac{I^{\text{eq}}(\eta')}{\mu} \exp\left(\frac{\eta' - \eta}{\mu}\right) d\eta', \quad -1 \leq \mu \leq 0, \end{aligned} \quad (\text{A1})$$

where $I^+(0, \mu)$ and $I^-(\xi, \mu)$ are determined by the boundary conditions

$$\begin{aligned} y = 0, \quad I^+(0, \mu) = & (1 - s)I^{\text{eq}}(T_h) + sI^-(0, -\mu), \\ y = d, \quad I^-(d, \mu) = & (1 - s)I^{\text{eq}}(T_c) + sI^+(d, -\mu). \end{aligned} \quad (\text{A2})$$

Here we show the determination of $I^+(0, \mu)$ in Eq. (A1), where $I^-(\xi, \mu)$ could be determined through similar

procedures. From the second equation in Eq. (A1), one obtains $I^-(0, -\mu)$ in the first boundary condition in Eq. (A2):

$$I^-(0, -\mu) = I^-(\xi, -\mu) \exp\left(-\frac{\xi}{\mu}\right) + \int_0^\xi \frac{I^{\text{eq}}(\eta')}{\mu} \exp\left(-\frac{\eta'}{\mu}\right) d\eta'. \quad (\text{A3})$$

From the second boundary condition in Eq. (A2), one could further get $I^-(\xi, -\mu)$ in Eq. (A3):

$$I^-(\xi, -\mu) = (1-s)I^{\text{eq}}(T_c) + sI^+(\xi, \mu). \quad (\text{A4})$$

Substituting Eq. (A4) into Eq. (A3), we get $I^-(0, -\mu)$ as below:

$$\begin{aligned} I^-(0, -\mu) &= [(1-s)I^{\text{eq}}(T_c) + sI^+(\xi, \mu)] \exp\left(-\frac{\xi}{\mu}\right) + \int_0^\xi \frac{I^{\text{eq}}(\eta')}{\mu} \exp\left(-\frac{\eta'}{\mu}\right) d\eta' \\ &= (1-s)I^{\text{eq}}(T_c) \exp\left(-\frac{\xi}{\mu}\right) + sI^+(\xi, \mu) \exp\left(-\frac{\xi}{\mu}\right) + \int_0^\xi \frac{I^{\text{eq}}(\eta')}{\mu} \exp\left(-\frac{\eta'}{\mu}\right) d\eta'. \end{aligned} \quad (\text{A5})$$

The $I^+(\xi, \mu)$ in Eq. (A5) can be obtained from the first equation in Eq. (A1):

$$I^+(\xi, \mu) = I^+(0, \mu) \exp\left(-\frac{\xi}{\mu}\right) + \int_0^\xi \frac{I^{\text{eq}}(\eta')}{\mu} \exp\left(\frac{\eta' - \xi}{\mu}\right) d\eta'. \quad (\text{A6})$$

Putting Eq. (A6) into Eq. (A5), we acquire $I^-(0, -\mu)$ as

$$\begin{aligned} I^-(0, -\mu) &= (1-s)I^{\text{eq}}(T_c) \exp\left(-\frac{\xi}{\mu}\right) + \int_0^\xi \frac{I^{\text{eq}}(\eta')}{\mu} \exp\left(-\frac{\eta'}{\mu}\right) d\eta' \\ &\quad + s \left[I^+(0, \mu) \exp\left(-\frac{\xi}{\mu}\right) + \int_0^\xi \frac{I^{\text{eq}}(\eta')}{\mu} \exp\left(\frac{\eta' - \xi}{\mu}\right) d\eta' \right] \exp\left(-\frac{\xi}{\mu}\right) \\ &= (1-s)I^{\text{eq}}(T_c) \exp\left(-\frac{\xi}{\mu}\right) + \int_0^\xi \frac{I^{\text{eq}}(\eta')}{\mu} \exp\left(-\frac{\eta'}{\mu}\right) d\eta' + sI^+(0, \mu) \exp\left(-\frac{2\xi}{\mu}\right) \\ &\quad + s \exp\left(-\frac{\xi}{\mu}\right) \int_0^\xi \frac{I^{\text{eq}}(\eta')}{\mu} \exp\left(\frac{\eta' - \xi}{\mu}\right) d\eta'. \end{aligned} \quad (\text{A7})$$

Substituting Eq. (A7) into the first boundary condition in Eq. (A2), we obtain an equation for $I^+(0, \mu)$:

$$\begin{aligned} I^+(0, \mu) &= (1-s)I^{\text{eq}}(T_h) + s(1-s)I^{\text{eq}}(T_c) \exp\left(-\frac{\xi}{\mu}\right) + s \int_0^\xi \frac{I^{\text{eq}}(\eta')}{\mu} \exp\left(-\frac{\eta'}{\mu}\right) d\eta' \\ &\quad + s^2 I^+(0, \mu) \exp\left(-\frac{2\xi}{\mu}\right) + s^2 \exp\left(-\frac{2\xi}{\mu}\right) \int_0^\xi \frac{I^{\text{eq}}(\eta')}{\mu} \exp\left(\frac{\eta'}{\mu}\right) d\eta'. \end{aligned} \quad (\text{A8})$$

Therefore, $I^+(0, \mu)$ is determined through a solution of Eq. (A8):

$$\begin{aligned} I^+(0, \mu) &= \frac{(1-s)}{1-s^2 \exp(-2\xi/\mu)} I^{\text{eq}}(T_h) + \frac{s(1-s)}{1-s^2 \exp(-2\xi/\mu)} I^{\text{eq}}(T_c) \exp\left(-\frac{\xi}{\mu}\right) \\ &\quad + \frac{s}{1-s^2 \exp(-2\xi/\mu)} \int_0^\xi \frac{I^{\text{eq}}(\eta')}{\mu} \exp\left(-\frac{\eta'}{\mu}\right) d\eta' + \frac{s^2 \exp(-2\xi/\mu)}{1-s^2 \exp(-2\xi/\mu)} \int_0^\xi \frac{I^{\text{eq}}(\eta')}{\mu} \exp\left(\frac{\eta'}{\mu}\right) d\eta'. \end{aligned} \quad (\text{A9})$$

APPENDIX B: NUMERICAL SOLUTION OF THE ENERGY DENSITY DISTRIBUTION IN CROSS-PLANE PHONON TRANSPORT THROUGH A THIN FILM

The integral equation for the energy density distribution is

$$2e^*(\eta) = G(\eta) + \int_0^\xi e^*(\eta') \int_0^1 F(\eta', \eta, \mu) d\mu d\eta'. \quad (\text{B1})$$

To avoid the numerical singularity in Eq. (B1) when $\eta = \eta'$, the following scheme is constructed similarly to the solution for the fully diffuse case [1]:

$$2e^*(\eta) = G(\eta) + \int_0^\xi [e^*(\eta') - e^*(\eta)] \int_0^1 F(\eta', \eta, \mu) d\mu d\eta' + e^*(\eta) \int_0^\xi \int_0^1 F(\eta', \eta, \mu) d\mu d\eta'. \quad (\text{B2})$$

The numerical singularity is eliminated since the first integral at the right-hand side of Eq. (B2) vanishes at $\eta = \eta'$. Equation (B2) is slightly reformulated as

$$[2 - c(\eta)]e^*(\eta) = G(\eta) + \int_0^\xi [e^*(\eta') - e^*(\eta)] \int_0^1 F(\eta', \eta, \mu) d\mu d\eta', \quad (\text{B3})$$

with $c(\eta) = \int_0^\xi \int_0^1 F(\eta', \eta, \mu) d\mu d\eta'$. The following trapezoidal integration formula is used for the integral in Eq. (B3):

$$\int_{x_1}^{x_n} f(x) dx = f(x_1) \frac{\Delta x}{2} + \Delta x \sum_{i=2}^{n-1} f(x_i) + f(x_n) \frac{\Delta x}{2}. \quad (\text{B4})$$

Therefore the discrete form of Eq. (B3) becomes

$$[2 - c(\eta_j)]e^*(\eta_j) = G(\eta_j) + \frac{\Delta\eta}{2}[e^*(\eta_1) - e^*(\eta_j)]F_{\text{int}}(\eta_1, \eta_j) + \Delta\eta \sum_{\substack{i=2 \\ i \neq j}}^{n-1} [e^*(\eta_i) - e^*(\eta_j)]F_{\text{int}}(\eta_i, \eta_j) \\ + \frac{\Delta\eta}{2}[e^*(\eta_n) - e^*(\eta_j)]F_{\text{int}}(\eta_n, \eta_j), \quad (\text{B5})$$

where the discrete coordinate points are $\eta_j = (\eta_1, \eta_2, \dots, \eta_n)$ with $n = N_\eta$, and a uniform integral interval is adopted: $\Delta\eta = \xi/(n-1)$. The integral function in Eq. (B5) is denoted fully as $F_{\text{int}}(\eta_i, \eta_j) = \int_0^1 F(\eta_i, \eta_j, \mu) d\mu$.

Equation (B5) is rewritten as the matrix multiplying form ($Ae^* = b$) as

$$\left[2 - c(\eta_j) + \frac{\Delta\eta}{2} F_{\text{int}}(\eta_1, \eta_j) + \Delta\eta \sum_{\substack{i=2 \\ i \neq j}}^{n-1} F_{\text{int}}(\eta_i, \eta_j) + \frac{\Delta\eta}{2} F_{\text{int}}(\eta_n, \eta_j) \right] e^*(\eta_j) \\ - \frac{\Delta\eta}{2} F_{\text{int}}(\eta_1, \eta_j) e^*(\eta_1) - \Delta\eta \sum_{\substack{i=2 \\ i \neq j}}^{n-1} F_{\text{int}}(\eta_i, \eta_j) e^*(\eta_i) - \frac{\Delta\eta}{2} F_{\text{int}}(\eta_n, \eta_j) e^*(\eta_n) = G(\eta_j). \quad (\text{B6})$$

A solution of Eq. (B6) by matrix inversion gives exactly the numerical results of energy density distribution $e^*(\eta_j)$.

APPENDIX C: LAPLACE TRANSFORM SOLUTION OF THE PHONON HYDRODYNAMIC MODEL FOR 1D TRANSIENT PHONON TRANSPORT ACROSS A THIN FILM

The Laplace transform of the temperature differential Eq. (89) for 1D transient phonon transport across a thin film is

$$p^2 \bar{\Theta}(X; p) + p \bar{\Theta}(X; p) \\ = \frac{1}{3} \text{Kn}_l^2 \frac{d^2 \bar{\Theta}(X; p)}{dX^2} + \frac{4}{15} \text{Kn}_l^2 p \frac{d \bar{\Theta}(X; p)}{dX}. \quad (\text{C1})$$

Equation (C1) is rewritten as an ordinary differential equation (ODE):

$$\frac{d^2 \bar{\Theta}(X; p)}{dX^2} = A^2 \bar{\Theta}(X; p), \quad (\text{C2})$$

with the parameter A fully expressed as

$$A \equiv \sqrt{\frac{p(p+1)}{\frac{1}{3} \text{Kn}_l^2 + \frac{4}{15} \text{Kn}_l^2 p}}. \quad (\text{C3})$$

The general solution of Eq. (C2) is

$$\bar{\Theta}(X; p) = C_1 \exp(AX) + C_2 \exp(-AX). \quad (\text{C4})$$

The coefficients C_1 and C_2 in Eq. (C4) are specified from the Laplace transform of the boundary conditions Eq. (90):

$$X = 0, \quad \bar{\Theta}(X; p) - \frac{1}{p} = \frac{2}{3} \text{Kn}_l \frac{d \bar{\Theta}(X; p)}{dX}, \\ X = 1, \quad \bar{\Theta}(X; p) = -\frac{2}{3} \text{Kn}_l \frac{d \bar{\Theta}(X; p)}{dX}. \quad (\text{C5})$$

Therefore, the coefficients C_1 and C_2 are determined as below:

$$C_1 = \frac{\frac{2}{3} \text{Kn}_l A - 1}{\left(\frac{2}{3} \text{Kn}_l A + 1\right)^2 \exp(2A) - \left(\frac{2}{3} \text{Kn}_l A - 1\right)^2} \frac{1}{p}, \quad (\text{C6})$$

$$C_2 = \frac{\left(\frac{2}{3} \text{Kn}_l A + 1\right) \exp(2A)}{\left(\frac{2}{3} \text{Kn}_l A + 1\right)^2 \exp(2A) - \left(\frac{2}{3} \text{Kn}_l A - 1\right)^2} \frac{1}{p}. \quad (\text{C7})$$

Thus Eq. (C4) with Eqs. (C3), (C6), (C7) constitute the solution of dimensionless temperature distribution in the frequency domain.

The solution of dimensionless heat flux distribution is related to that of the dimensionless temperature distribution based on the Laplace transform of Eq. (87) and Eq. (88):

$$p \bar{q}^*(X; p) + \bar{q}^*(X; p) \\ = -\frac{1}{3} \text{Kn}_l \frac{d \bar{\Theta}(X; p)}{dX} + \frac{4}{15} \text{Kn}_l^2 \frac{d^2 \bar{q}^*(X; p)}{dX^2}, \quad (\text{C8})$$

$$p \bar{\Theta}(X; p) = -\text{Kn}_l \frac{d \bar{q}^*(X; p)}{dX}. \quad (\text{C9})$$

From Eq. (C8) and Eq. (C9), one could derive the following relation:

$$\bar{q}^*(X; p) = -B \frac{d\bar{\Theta}(X; p)}{dX}, \quad (\text{C10})$$

where the parameter B is denoted fully as

$$B \equiv \frac{\frac{1}{3}\text{Kn}_l + \frac{4}{15}p\text{Kn}_l}{1 + p}. \quad (\text{C11})$$

Substituting Eq. (C4) into Eq. (C10), we acquire the solution of the dimensionless heat flux distribution in the frequency domain:

$$\bar{q}^*(X; p) = -B[C_1 A \exp(AX) - C_2 A \exp(-AX)]. \quad (\text{C12})$$

To get the temporal evolutions of the dimensionless temperature distribution and heat flux distribution in the real domain, we apply an inverse Laplace transform based on the following Riemann-sum approximation [83]:

$$\begin{aligned} \Theta(X, \tau) &\simeq \frac{\exp(\gamma\tau)}{\tau} \left[\frac{1}{2} \bar{\Theta}(X; \gamma) + \text{Re} \sum_{n=1}^{\infty} \bar{\Theta}\left(X; \gamma + \frac{in\pi}{\tau}\right) (-1)^n \right], \\ & \quad (\text{C13}) \end{aligned}$$

$$\begin{aligned} q^*(X, \tau) &\simeq \frac{\exp(\gamma\tau)}{\tau} \left[\frac{1}{2} \bar{q}^*(X; \gamma) + \text{Re} \sum_{n=1}^{\infty} \bar{q}^*\left(X; \gamma + \frac{in\pi}{\tau}\right) (-1)^n \right], \\ & \quad (\text{C14}) \end{aligned}$$

where $\gamma\tau = 3$, and ‘‘Re’’ denotes the real part of a complex variable, with i the imaginary index.

APPENDIX D: LAPLACE TRANSFORM SOLUTION OF THE PHONON HYDRODYNAMIC MODEL FOR HIGH-FREQUENCY PERIODIC HEATING OF A SEMI-INFINITE SURFACE

The Laplace transform of the temperature differential Eq. (95) gives rises to an ordinary differential equation (ODE):

$$\frac{d^2\bar{\Theta}(X; p)}{dX^2} = A^2\bar{\Theta}(X; p), \quad (\text{D1})$$

with the parameter A fully denoted as

$$A \equiv \sqrt{\frac{p(p+1)}{\frac{1}{3} + \frac{4}{15}p}}. \quad (\text{D2})$$

The general solution of Eq. (D1) is

$$\bar{\Theta}(X; p) = C_1 \exp(AX) + C_2 \exp(-AX), \quad (\text{D3})$$

where the coefficients C_1 and C_2 are determined from the Laplace transform of the boundary conditions Eq. (96):

$$\begin{aligned} X = 0, \quad \bar{\Theta}(X; p) - \frac{2}{3} \frac{d\bar{\Theta}(X; p)}{dX} &= \frac{p}{p^2 + (\text{Kn}_l)^2}, \\ X \rightarrow \infty, \quad \bar{\Theta}(X; p) &= 0. \end{aligned} \quad (\text{D4})$$

From the second boundary condition in Eq. (D4), one could get $C_1 = 0$. With the aid of the first boundary condition, the other coefficient is specified as

$$C_2 = \frac{1}{1 + \frac{2}{3}A} \frac{p}{p^2 + (\text{Kn}_l)^2}. \quad (\text{D5})$$

Therefore, the dimensionless temperature distribution in the frequency domain is obtained as

$$\bar{\Theta}(X; p) = \frac{1}{1 + \frac{2}{3}A} \frac{p}{p^2 + (\text{Kn}_l)^2} \exp(-AX). \quad (\text{D6})$$

Through similar procedures in Appendix C, the dimensionless heat flux distribution is related to the dimensionless temperature distribution as

$$\bar{q}^*(X; p) = -B \frac{d\bar{\Theta}(X; p)}{dX}, \quad (\text{D7})$$

with the parameter B fully denoted as

$$B \equiv \frac{\frac{1}{3} + \frac{4}{15}p}{1 + p}. \quad (\text{D8})$$

Putting Eq. (D6) into Eq. (D7), we get the dimensionless heat flux distribution in the frequency domain as

$$\bar{q}^*(X; p) = C_2 AB \exp(-AX). \quad (\text{D9})$$

Finally, the temporal evolutions of the dimensionless temperature distribution and heat flux distribution are obtained through an inverse Laplace transform based on the Riemann-sum approximation Eqs. (C13) and (C14).

[1] G. Chen, *Nanoscale Energy Transport and Conversion: A Parallel Treatment of Electrons, Molecules, Phonons, and Photons* (Oxford University Press, New York, 2005).
 [2] D. G. Cahill, P. V. Braun, G. Chen, D. R. Clarke, S. Fan, K. E. Goodson, P. Keblinski, W. P. King, G. D. Mahan, A. Majumdar, H. J. Maris, S. R. Phillpot, E. Pop, and L. Shi, Nanoscale thermal transport. II. 2003–2012, *Appl. Phys. Rev.* **1**, 011305 (2014).
 [3] Y. Guo and M. Wang, Phonon hydrodynamics and its applications in nanoscale heat transport, *Phys. Rep.* **595**, 1 (2015).

[4] A. J. Minnich, M. S. Dresselhaus, Z. F. Ren, and G. Chen, Bulk nanostructured thermoelectric materials: Current research and future prospects, *Energy Environ. Sci.* **2**, 466 (2009).
 [5] S. I. Kim, K. H. Lee, H. A. Mun, H. S. Kim, S. W. Hwang, J. W. Roh, D. J. Yang, W. H. Shin, X. S. Li, and Y. H. Lee, Dense dislocation arrays embedded in grain boundaries for high-performance bulk thermoelectrics, *Science* **348**, 109 (2015).
 [6] A. L. Moore and L. Shi, Emerging challenges and materials for thermal management of electronics, *Mater. Today* **17**, 163 (2014).

- [7] J. Schlee, J. Mateos, I. Íñiguez-de-La-Torre, N. Wadefalk, P. Nilsson, J. Grahn, and A. Minnich, Phonon black-body radiation limit for heat dissipation in electronics, *Nat. Mater.* **14**, 187 (2015).
- [8] R. R. Gattass and E. Mazur, Femtosecond laser micromachining in transparent materials, *Nat. Photonics* **2**, 219 (2008).
- [9] P. Ji and Y. Zhang, Electron-phonon coupled heat transfer and thermal response induced by femtosecond laser heating of gold, *J. Heat Transfer* **139**, 052001 (2017).
- [10] D. A. Broido, M. Malorny, G. Birner, N. Mingo, and D. A. Stewart, Intrinsic lattice thermal conductivity of semiconductors from first principles, *Appl. Phys. Lett.* **91**, 231922 (2007).
- [11] L. Lindsay, First principles Peierls-Boltzmann phonon thermal transport: A topical review, *Nanoscale Microscale Thermophys. Eng.* **20**, 67 (2016).
- [12] N. Yang, G. Zhang, and B. Li, Violation of Fourier's law and anomalous heat diffusion in silicon nanowires, *Nano Today* **5**, 85 (2010).
- [13] A. J. H. McGaughey and J. M. Larkin, Predicting phonon properties from equilibrium molecular dynamics simulations, *Annu. Rev. Heat Transfer* **17**, 49 (2014).
- [14] A. J. H. McGaughey and M. Kaviani, Quantitative validation of the Boltzmann transport equation phonon thermal conductivity model under the single-mode relaxation time approximation, *Phys. Rev. B* **69**, 094303 (2004).
- [15] J. V. Goicochea, M. Madrid, and C. Amon, Hierarchical modeling of heat transfer in silicon-based electronic devices, *J. Heat Transfer* **132**, 102401 (2010).
- [16] J. Cuffe, J. K. Eliason, A. A. Maznev, K. C. Collins, J. A. Johnson, A. Shchepetov, M. Prunnila, J. Ahopelto, C. M. S. Torres, and G. Chen, Reconstructing phonon mean-free-path contributions to thermal conductivity using nanoscale membranes, *Phys. Rev. B* **91**, 245423 (2015).
- [17] G. Chen, Multiscale simulation of phonon and electron thermal transport, *Annu. Rev. Heat Transfer* **17**, 1 (2014).
- [18] D. Y. Tzou, A unified field approach for heat conduction from macro- to micro-scales, *J. Heat Transfer* **117**, 8 (1995).
- [19] F. X. Alvarez, D. Jou, and A. Sellitto, Phonon hydrodynamics and phonon-boundary scattering in nanosystems, *J. Appl. Phys.* **105**, 014317 (2009).
- [20] M. Wang, N. Yang, and Z.-Y. Guo, Non-Fourier heat conductions in nanomaterials, *J. Appl. Phys.* **110**, 064310 (2011).
- [21] J. Maassen and M. Lundstrom, Steady-state heat transport: Ballistic-to-diffusive with Fourier's law, *J. Appl. Phys.* **117**, 035104 (2015).
- [22] D. D. Joseph and L. Preziosi, Heat waves, *Rev. Mod. Phys.* **61**, 41 (1989).
- [23] R. A. Guyer and J. A. Krumhansl, Thermal conductivity, second sound, and phonon hydrodynamic phenomena in nonmetallic crystals, *Phys. Rev.* **148**, 778 (1966).
- [24] R. A. Guyer and J. A. Krumhansl, Solution of the linearized phonon Boltzmann equation, *Phys. Rev.* **148**, 766 (1966).
- [25] W. Dreyer and H. Struchtrup, Heat pulse experiments revisited, *Continuum Mech. Therm.* **5**, 3 (1993).
- [26] M. J. Fryer and H. Struchtrup, Moment model and boundary conditions for energy transport in the phonon gas, *Continuum Mech. Therm.* **26**, 593 (2014).
- [27] F. X. Alvarez, D. Jou, and A. Sellitto, Pore-size dependence of the thermal conductivity of porous silicon: A phonon hydrodynamic approach, *Appl. Phys. Lett.* **97**, 033103 (2010).
- [28] A. Sellitto, F. X. Alvarez, and D. Jou, Second law of thermodynamics and phonon-boundary conditions in nanowires, *J. Appl. Phys.* **107**, 064302 (2010).
- [29] A. Sellitto, F. X. Alvarez, and D. Jou, Temperature dependence of boundary conditions in phonon hydrodynamics of smooth and rough nanowires, *J. Appl. Phys.* **107**, 114312 (2010).
- [30] Y. Ma, Size-dependent thermal conductivity in nanosystems based on non-Fourier heat transfer, *Appl. Phys. Lett.* **101**, 211905 (2012).
- [31] V. A. Cimmelli, A. Sellitto, and D. Jou, Nonlocal effects and second sound in a nonequilibrium steady state, *Phys. Rev. B* **79**, 014303 (2009).
- [32] V. A. Cimmelli, A. Sellitto, and D. Jou, Nonequilibrium temperatures, heat waves, and nonlinear heat transport equations, *Phys. Rev. B* **81**, 054301 (2010).
- [33] V. A. Cimmelli, A. Sellitto, and D. Jou, Nonlinear evolution and stability of the heat flow in nanosystems: Beyond linear phonon hydrodynamics, *Phys. Rev. B* **82**, 184302 (2010).
- [34] D. Jou, J. Casas-Vázquez, and G. Lebon, *Extended Irreversible Thermodynamics* (Springer, Heidelberg, 2010).
- [35] A. Sellitto, V. A. Cimmelli, and D. Jou, *Mesoscopic Theories of Heat Transport in Nanosystems* (Springer, Heidelberg, 2016).
- [36] G. Chen, Ballistic-Diffusive Heat-Conduction Equations, *Phys. Rev. Lett.* **86**, 2297 (2001).
- [37] C. V. Anderson and K. K. Tamma, Novel Heat Conduction Model for Bridging Different Space and Time Scales, *Phys. Rev. Lett.* **96**, 184301 (2006).
- [38] A. T. Ramu and Y. Ma, An enhanced Fourier law derivable from the Boltzmann transport equation and a sample application in determining the mean-free path of nondiffusive phonon modes, *J. Appl. Phys.* **116**, 093501 (2014).
- [39] J.-P. M. Péraud and N. G. Hadjiconstantinou, Extending the range of validity of Fourier's law into the kinetic transport regime via asymptotic solution of the phonon Boltzmann transport equation, *Phys. Rev. B* **93**, 045424 (2016).
- [40] A. Mohammadzadeh and H. Struchtrup, A moment model for phonon transport at room temperature, *Continuum Mech. Therm.* **29**, 117 (2017).
- [41] M. Kaviani, *Heat Transfer Physics* (Cambridge University Press, New York, 2014).
- [42] R. E. Peierls, *Quantum Theory of Solids* (Clarendon Press, Oxford, 1955).
- [43] J. Callaway, Model for lattice thermal conductivity at low temperatures, *Phys. Rev.* **113**, 1046 (1959).
- [44] Z. Banach and W. Larecki, Nine-moment phonon hydrodynamics based on the modified Grad-type approach: Formulation, *J. Phys. A: Math. Gen.* **37**, 9805 (2004).
- [45] Z. Banach and W. Larecki, Chapman-Enskog method for a phonon gas with finite heat flux, *J. Phys. A: Math. Theor.* **41**, 375502 (2008).
- [46] W. Li, N. Mingo, L. Lindsay, D. A. Broido, D. A. Stewart, and N. A. Katcho, Thermal conductivity of diamond nanowires from first principles, *Phys. Rev. B* **85**, 195436 (2012).
- [47] A. Cepellotti, G. Fugallo, L. Paulatto, M. Lazzeri, F. Mauri, and N. Marzari, Phonon hydrodynamics in two-dimensional materials, *Nat. Commun.* **6**, 6400 (2015).

- [48] S. Lee, D. Broido, K. Esfarjani, and G. Chen, Hydrodynamic phonon transport in suspended graphene, *Nat. Commun.* **6**, 6290 (2015).
- [49] Y. Guo and M. Wang, Heat transport in two-dimensional materials by directly solving the phonon Boltzmann equation under Callaway's dual relaxation model, *Phys. Rev. B* **96**, 134312 (2017).
- [50] A. Majumdar, Microscale heat conduction in dielectric thin films, *J. Heat Transfer* **115**, 7 (1993).
- [51] J.-P. M. Péraud and N. G. Hadjiconstantinou, Efficient simulation of multidimensional phonon transport using energy-based variance-reduced Monte Carlo formulations, *Phys. Rev. B* **84**, 205331 (2011).
- [52] S. Chapman and T. G. Cowling, *The Mathematical Theory of Nonuniform Gases* (Cambridge University Press, Cambridge, 1953).
- [53] H. Grad, On the kinetic theory of rarefied gases, *Commun. Pure Appl. Math.* **2**, 331 (1949).
- [54] H. Struchtrup, *Macroscopic Transport Equations for Rarefied Gas Flows* (Springer-Verlag, Heidelberg, 2005).
- [55] H. Struchtrup and M. Torrilhon, Regularization of Grad's 13 moment equations: Derivation and linear analysis, *Phys. Fluids* **15**, 2668 (2003).
- [56] M. Torrilhon, Modeling nonequilibrium gas flow based on moment equations, *Annu. Rev. Fluid Mech.* **48**, 429 (2016).
- [57] A. N. Gorban and I. V. Karlin, *Invariant Manifolds for Physical and Chemical Kinetics* (Springer, Heidelberg, 2005).
- [58] G. M. Kremer, *An Introduction to the Boltzmann Equation and Transport Processes in Gases* (Springer-Verlag, Heidelberg, 2010).
- [59] D. Y. Tzou, Nonlocal behavior in phonon transport, *Int. J. Heat Mass Transfer* **54**, 475 (2011).
- [60] Y. Ma, A transient ballistic-diffusive heat conduction model for heat pulse propagation in nonmetallic crystals, *Int. J. Heat Mass Transfer* **66**, 592 (2013).
- [61] W. Larecki and Z. Banach, Influence of nonlinearity of the phonon dispersion relation on wave velocities in the four-moment maximum entropy phonon hydrodynamics, *Physica D* **266**, 65 (2014).
- [62] G. Karniadakis, A. Beskok, and N. Aluru, *Microflows and Nanoflows: Fundamentals and Simulation* (Springer, New York, 2005).
- [63] M. Xu, Slip boundary condition of heat flux in Knudsen layers, *Proc. R. Soc. A* **470**, 20130578 (2014).
- [64] M. Torrilhon and H. Struchtrup, Boundary conditions for regularized 13-moment-equations for micro-channel-flows, *J. Comput. Phys.* **227**, 1982 (2008).
- [65] C. Cercignani, *The Boltzmann Equation and its Applications* (Springer-Verlag, New York, 1988).
- [66] N. K. Ravichandran and A. J. Minnich, Role of thermalizing and nonthermalizing walls in phonon heat conduction along thin films, *Phys. Rev. B* **93**, 035314 (2016).
- [67] J. E. Turney, A. J. H. McGaughey, and C. H. Amon, In-plane phonon transport in thin films, *J. Appl. Phys.* **107**, 024317 (2010).
- [68] D. P. Sellan, J. E. Turney, A. J. H. McGaughey, and C. H. Amon, Cross-plane phonon transport in thin films, *J. Appl. Phys.* **108**, 113524 (2010).
- [69] Y.-C. Hua and B.-Y. Cao, Phonon ballistic-diffusive heat conduction in silicon nanofilms by Monte Carlo simulations, *Int. J. Heat Mass Transfer* **78**, 755 (2014).
- [70] K. T. Regner, D. P. Sellan, Z. H. Su, C. H. Amon, A. J. H. McGaughey, and J. A. Malen, Broadband phonon mean free path contributions to thermal conductivity measured using frequency domain thermoreflectance, *Nat. Commun.* **4**, 1640 (2013).
- [71] F. Yang and C. Dames, Heating-frequency-dependent thermal conductivity: An analytical solution from diffusive to ballistic regime and its relevance to phonon scattering measurements, *Phys. Rev. B* **91**, 165311 (2015).
- [72] J. A. Johnson, A. Maznev, J. Cuffe, J. K. Eliason, A. J. Minnich, T. Kehoe, C. M. S. Torres, G. Chen, and K. A. Nelson, Direct Measurement of Room-Temperature Nondiffusive Thermal Transport over Micron Distances in a Silicon Membrane, *Phys. Rev. Lett.* **110**, 025901 (2013).
- [73] M. Asheghi, M. N. Touzelbaev, K. E. Goodson, Y. K. Leung, and S. S. Wong, Temperature-dependent thermal conductivity of single-crystal silicon layers in SOI substrates, *J. Heat Transfer* **120**, 30 (1998).
- [74] Y. S. Ju and K. E. Goodson, Phonon scattering in silicon films with thickness of order 100 nm, *Appl. Phys. Lett.* **74**, 3005 (1999).
- [75] W. Liu and M. Asheghi, Phonon-boundary scattering in ultrathin single-crystal silicon layers, *Appl. Phys. Lett.* **84**, 3819 (2004).
- [76] E. Chávez-Ángel, J. Reparaz, J. Gomis-Bresco, M. Wagner, J. Cuffe, B. Graczykowski, A. Shchepetov, H. Jiang, M. Prunnila, and J. Ahopelto, Reduction of the thermal conductivity in free-standing silicon nano-membranes investigated by non-invasive Raman thermometry, *APL Mater.* **2**, 012113 (2014).
- [77] F. Yang and C. Dames, Mean free path spectra as a tool to understand thermal conductivity in bulk and nanostructures, *Phys. Rev. B* **87**, 035437 (2013).
- [78] C. Hua and A. J. Minnich, Semi-analytical solution to the frequency-dependent Boltzmann transport equation for cross-plane heat conduction in thin films, *J. Appl. Phys.* **117**, 175306 (2015).
- [79] Y. Guo and M. Wang, Lattice Boltzmann modeling of phonon transport, *J. Comput. Phys.* **315**, 1 (2016).
- [80] R. Dingle, The electrical conductivity of thin wires, *Proc. R. Soc. London A* **201**, 545 (1950).
- [81] Y. Zhang and W. Ye, Modified ballistic-diffusive equations for transient non-continuum heat conduction, *Int. J. Heat Mass Transfer* **83**, 51 (2015).
- [82] J.-P. M. Péraud and N. G. Hadjiconstantinou, An alternative approach to efficient simulation of micro/nanoscale phonon transport, *Appl. Phys. Lett.* **101**, 153114 (2012).
- [83] D. Y. Tzou, *Macro- to Microscale Heat Transfer: The Lagging Behavior* (John Wiley & Sons, Ltd., Chichester, 2015).
- [84] L. P. Zeng, V. Chiloyan, S. Huberman, A. A. Maznev, J.-P. M. Péraud, N. G. Hadjiconstantinou, K. A. Nelson, and G. Chen, Monte Carlo study of non-diffusive relaxation of a transient thermal grating in thin membranes, *Appl. Phys. Lett.* **108**, 063107 (2016).